Facies control on seismites in an alluvial–aeolian system: The Pliocene dunefield of the Teruel half-graben basin (eastern Spain)

Carlos L. Liesa [a], Juan Pedro Rodríguez-López [b], Lope Ezquerro [a], Pedro Alfaro [c], Miguel Ángel Rodríguez-Pascua [d], Paloma Lafuente [a], Luis Arlegui [a], José L. Simón [a]

[a] Grupo GEOTRANSFER, Área de Geodinámica Interna, Departamento de Ciencias de la Tierra, Facultad de Ciencias, Universidad de Zaragoza, C/ Pablo Cerbuna 12, 50009 Zaragoza, Spain
[b] School of Applied Sciences, Faculty of Computing, Engineering and Science, University of South Wales, CF37 1DL, Pontypridd, Wales, UK
[c] Departamento de Ciencias de la Tierra y del Medio Ambiente, Facultad de Ciencias, Universidad de Alicante, 03080 Alicante, Spain
[d] Instituto Geológico y Minero de España, C/ Ríos Rosas 23, 28003 Madrid, Spain

A B S T R A C T

The recognition of seismically induced soft-sediment deformation structures (SSDS) in sedimentary successions characterized by different facies, and hence by different rheology, is challenging. This is the case for high porosity and high permeability aeolian facies interbedded with muddy wet interdune deposits and alluvial conglomerates and sandstones. Several types of SSDS have been studied in two exposures of the Upper Pliocene (2.9–2.6 Ma) sediments of a fault-bounded intracontinental aeolian dune field in the Teruel Basin (Iberian Chain, eastern Spain). Among SSDS, load and fluid-escape structures, apart from several animal tracks, have been recognized. Those structures show an irregular distribution through the studied stratigraphic sections, being scarce in homogenous aeolian sands and frequent in water-related facies. A detailed study of the distribution and geometry of SSDS and their relationships with respect to the stratigraphic architecture and facies has allowed a critical discrimination of trigger mechanisms, i.e. biological or physical overloading vs. earthquakes. The seismically induced structures are concentrated into seven deformed beds, showing an uneven lateral distribution and geometry closely controlled by the hosting sedimentary facies and their rheology. These seismites resulted from liquefaction during moderate earthquakes (estimated magnitude from 5.0 to 6.8). The most probable seismogenic source was the Sierra del Pobo normal fault zone, located 2 km to the East. Results show how an appropriate recognition of sedimentary facies is crucial to understand the lateral variability of seismites in sedimentary environments characterized by sharp facies changes.

1. Introduction

The Teruel Basin is one of the main extensional features of the Iberian Chain developed during the Neogene and the Quaternary. Its tectonic activity is continuous at present, in a radial extensional stress field (Simón, 1989; Liesa, 2000, 2011; Arlegui et al., 2005, 2006). Several normal faults or fault zones accommodate this extension: Sierra del Pobo, Concud or Sierra de Palomera faults, among others (Gutiérrez et al., 2012; Simón et al., 2012).

This tectonic activity results in a moderate seismicity (Lafuente et al., 2011, 2014). Evidences of significant paleoearthquakes have been described in detail in the Concud Fault (Gutiérrez et al., 2008; Lafuente et al., 2011, 2014). In addition, seismites in Pliocene and Pleistocene sediments of the Teruel Basin were analyzed by Lafuente et al. (2008).

The identification of seismites (sensu Seilacher, 1969) is important because they have significant implications for syntectonic sedimentary basins, especially in an area of moderate seismic activity such as the Teruel Basin. Although significant progress has been made to understand the processes that trigger soft-sediment deformation, the interpretation is not an easy task (see discussion in Owen et al., 2011) and their recognition and interpretation can be challenging due to quick lateral variability of sedimentary facies associated with a particular deformation level (e.g. Rodríguez-López et al., 2007).

Two short stratigraphic sections of an Upper Pliocene dune field (Escorihuela Formation) in the Teruel Basin (Iberian Chain, eastern Spain) have been studied in detail. This succession is prolix in soft-sediment deformation structures (SSDS), and different triggers have been proposed for them. Lafuente et al. (2008) only focused on seismically induced SSDS, while Rodríguez-López et al. (2012a) also recognized the occurrence of mammal footprints. This paper deals with a detailed description and analysis of SSDS, trying to identify

E-mail address: carluis@unizar.es (C.L. Liesa).

seismites and understand the relationship of SSDS geometry and distribution with the involved sedimentary facies. In order to identify trigger mechanisms, we apply the three-stage approach proposed by Owen et al. (2011). As the understanding of the depositional palaeoenvironment is essential for trigger interpretation, this study also includes an exhaustive evaluation and analysis of the sedimentary facies involved during deformation. The control of the sedimentary facies and palaeoenvironments on the lateral distribution of deformation structures and their morphological features is also discussed.

2. Geological setting

The Teruel Basin is located in the northeastern part of the Iberian Peninsula, in the central-eastern Iberian Chain (Fig. 1A and B). This NNE-SSW trending basin is transverse to the NW-SE structural trend

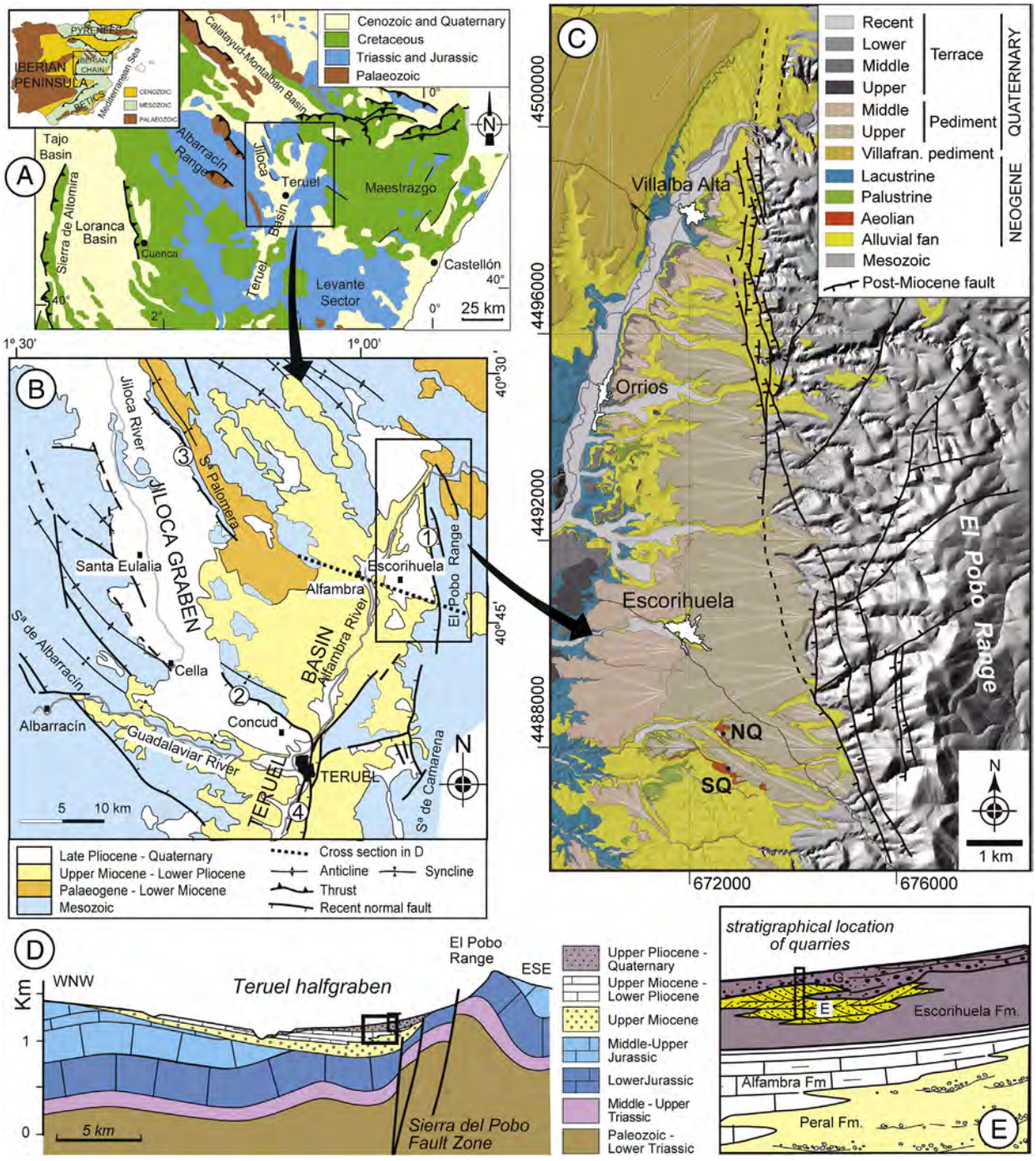

Fig. 1. Geological location of the study area. (A) Location of the NNE-SSW Teruel Basin in central-eastern Iberian Chain (NE Spain). Note its transverse trend with respect to the main NW-SE structural trend of the Iberian Chain. Inset shows its location within Iberia. (B) Geological map of the northern part of the Teruel Basin with the location of the study area (modified from Rubio and Simón, 2007): 1—El Pobo Fault System, 2—Concud Fault, 3—Sierra de Palomera Fault, and 4—Teruel Fault. (C) Geological map of the studied area showing the location of studied sections near Escorihuela (NQ—North Quarry, SQ—South Quarry) and the Sierra del Pobo fault zone. (D) Simplified geological cross-section (see B for location) showing the half-graben structure of the Teruel Basin in the Escorihuela sector. (E) Scheme (without scale) with the Neogene–Quaternary lithological units cropping out at the Escorihuela sector (see location in B–C): Peral Formation (Vallesian, Late Miocene), Alfambra Fm. (Late Miocene–Early Pliocene), Escorihuela Fm (Middle–Late Pliocene), in which the aeolian-fluvial deposits (E), and Late Pliocene–Quaternary (Pleistocene, Villafranchian) pediment (glacis) deposits (G) are indicated. (D) and (E) modified from Lafuente et al. (2008).

of the mainly Palaeogene Iberian Chain (Capote et al., 2002; Liesa and Simón, 2009) (Fig. 1A and B). It developed during the Miocene–Pliocene rifting stage that affected the eastern margin of Iberia and formed the Valencia through (e.g., Álvaro et al., 1979; Vegas et al., 1979; Simón, 1982; Roca and Guimerà, 1992).

The Teruel Basin was filled by a rather complete Neogene succession up to 500 m thick (Moissenet, 1983, 1989). At the northern sector, where the studied area is located (Fig. 1B), the infill ranges from the Late Miocene (Vallesian) to the Late Pliocene (Villafranchian) in age (Alcalá et al., 2000; Alonso-Zarza and Calvo, 2000), and comprises four stratigraphic units (van de Weerd, 1976): the Peral, Alfambra, Tortajada, and Escorihuela Formations (Fig. 1E). They were covered by Pleistocene (pediment) gravel deposits (Fig. 1E) sourced at the Sierra del Pobo highland. Then, three levels of stepped glacis-terrace systems developed during the Quaternary (Gutiérrez and Peña, 1976).

The Escorihuela Formation (van de Weerd, 1976) is a 30- to 35-m-thick succession mainly formed by brown sands, grey clays, and white limestone beds. This unit correlates laterally with the unit 'Rojo 3' by Godoy et al. (1983), the unit V by Alcalá et al. (2000) and Alonso-Zarza and Calvo (2000), and the megasequence 5 by Ezquerro et al. (2014). It is Middle–Late Pliocene to Early Pleistocene in age, based on mammal faunas (van de Weerd, 1976; van Dam, 1997; Alcalá et al., 2000; van Dam et al., 2006) and magnetostratigraphy (Opdyke et al., 1997; Alcalá et al., 2000; Garcés et al., 1999; van Dam et al., 2001; Ezquerro et al., 2012).

This manuscript focuses on the soft-sediment deformation structures recognized at the upper part of the Escorihuela Formation, which is characterized by fine-grained to coarse-grained and well-sorted sandstones and interbedded conglomerates (Fig. 1E) (e.g. Gutiérrez and Peña, 1976; Carrillo and Gisbert, 1979). These sediments have been recently interpreted by Rodríguez-López et al. (2012a) as deposited within an aeolian dunefield laterally interfingering with alluvial fans fed from the footwall highlands of the active El Pobo normal fault zone (Figs. 1B, C, and D). The Escorihuela Formation also interfingers and shows a gradual transition with the overlying *Villafranchian pediment* unit (Ezquerro et al., 2012; Rodríguez-López et al., 2012a).

The northern sector of the Teruel basin is a half-graben bounded by the N-S striking Sierra del Pobo fault zone (Fig. 1C). A gentle roll-over monocline linked to this fault zone is expressed as eastwards tilting of most of the Neogene basin infill (1–2°, in average), except for a fringe at the eastern margin where westwards dipping is observed completing a gentle asymmetric syncline (Fig. 1D). The eastwards tilting also affects a planation surface (*Fundamental Erosion Surface*, as defined by Peña et al., 1984) correlative of the uppermost lacustrine deposits of the Alfambra Formation, which extends westwards truncating Mesozoic and Palaeogene materials up to Sierra Palomera (Fig. 1C and D). Based on this composite, sedimentary, and geomorphological marker (Early Pliocene in age, latest Ruscinian: Godoy et al., 1983; Opdyke et al., 1997; Alcalá et al., 2000), an offset of ~400 m has been inferred for the Sierra del Pobo fault zone for the last 3.6 Ma, therefore an average vertical slip rate of about 0.11 mm/a (Simón et al., 2012). These values allow characterizing this structure as a moderately active fault during Late Pliocene–Quaternary times.

The Sierra del Pobo fault zone depicts, at surface, a number of anastomosing fault traces trending around N-S (Fig. 1C). All the individual fault surfaces probably coalesce at depth (Fig. 1D) into a single crustal fault that could attain the 11- to 14-km-deep detachment level proposed by Roca and Guimerà (1992) for the overall eastern Iberian extensional system. The minimum length of this active structure is 14.5 km (perhaps reaching 16 km), seeing at the nearly continuous trace of the western branch (Fig. 1C). Introducing this parameter into empirical relationships proposed by Wells and Coppersmith (1994), Stirling et al. (2002), and Pavlides and Caputo (2004), we estimate a moment magnitude (Mw) for its potential earthquake in the range of 6.4–6.8, similar to that assigned (6.5 ± 0.37) in the Quaternary Active Fault Database of the Iberian Peninsula (QAFI; IGME, 2012).

3. The Pliocene continental depositional system of the Teruel Basin

Aeolian dunefields constitute sensitive depositional systems in which allocyclic controls are normally well recorded if an effective preservation of accumulated aeolian climbing system occurs (Rodríguez-López et al., 2014). The Pliocene aeolian dunefield of the Teruel Basin constitutes an excellent example of a synrift aeolian system associated with a variable phreatic level and intermittently affected by floods. The aeolian system recorded in the Escorihuela Formation is similar to other arid to semi-arid dunefields developed in half-graben basins where aeolian and water-laid sediments accumulate in association with the activity of extensional border faults (Rodríguez-López et al., 2012a and references therein).

Pliocene palaeowinds blew from the west moving the dune field perpendicular to the N-S trending border-fault, thus encroaching upon the associated alluvial fan relief to the east. Flooding waters coming from the alluvial fans met the encroaching aeolian dunefields leading to the intense reworking of aeolian sands and generating an overall stratigraphy characterized by interbedded alluvial and aeolian facies (Rodríguez-López et al., 2012a). The development and accumulation of the Escorihuela dune field (2.9–2.6 Ma) correlates with the expansion of other aeolian dune fields worldwide (e.g., Atacama, Namib, and Sahara deserts) during a strong and presumably regionally dry 400-kyr eccentricity minimum (2.8–2.7 Ma), and with the onset of the Northern-Hemisphere glaciation leading to stronger westerlies (Rodríguez-López et al., 2012a).

The facies, facies associations, as well as the stratigraphic architecture of the Pliocene deposits, have been presented in detail by Rodríguez-López et al. (2012a). This chapter displays a summary of the main characteristics of the aeolian and alluvial depositional systems in order to facilitate the understanding of the facies and their lateral and vertical relationships involved in the studied soft-sediment deformation structures. All the alluvial, fluvial, and aeolian facies associations are summarized in Table 1.

3.1. Aeolian depositional system

Wind-related deposits in the Pliocene of the Teruel Basin include aeolian dune (AD), aeolian sandsheets (ASS), low-angle aeolian (LA-A) deposits, and damp (DI) and wet interdune (WI) deposits (see Rodríguez-López et al., 2012a) (Table 1). Most of these aeolian facies are constituted by pale to yellow, fine- to coarse-grained sandstones with a variable occurrence of frosted dark granules normally accumulated at the aeolian dune bottomsets and deflation lags in both aeolian sandsheets and low-angle aeolian facies associations (Rodríguez-López et al., 2012a).

Aeolian dunes exhibit medium to large-scale trough cross-bedding contained in tabular and laterally continuous strata separated by aeolian superimposition surfaces (e.g. Mountney, 2006a). Foresets display concave-up and downwind dipping surfaces showing clear pinch outs between grainflow deposits and toe-set wind ripple lamination (cf. Hunter, 1977). Low-angle aeolian deposits are similar to those described by Kocurek (1986), with wind ripple lamination and granule-rich horizons, granule veneers or granule linings (cf. Rodríguez-López et al., 2010, 2012a). Aeolian sandsheet facies association is formed by m-thick intervals of fine-grained very well-sorted finely laminated sandstones showing subcritically climbing translatent strata with inverse grading and pin-stripe lamination (cf. Fryberger et al., 1983; Fryberger and Schenk, 1988). It is also characterized by adhesion lamination, bimodal deposits, deflation lags and granule ripples (Rodríguez-López et al., 2012a). These aeolian sandsheets underwent periods of accumulation, deflation, and stabilization, the last ones characterized by horizons showing calcitized roots. Damp interdunes are constituted by medium- to coarse-grained sands, with crinkly and irregular lamination, that accumulated at the dune aprons, which were in direct contact with the phreatic level (e.g. Mountney and

Table 1
Main facies associations (FA) distinguished in the aeolian and alluvial sedimentary systems of the Pliocene Escorihuela dunefield (modified from Rodríguez-López et al., 2012a).

FA and code	Lithology and geometry	Sedimentary structures	References
Aeolian system			
Aeolian dune AD	Pale to yellow fine- to coarse-grained sandstones. Tabular, laterally continuous bodies.	Large-scale trough cross-bedded sets; aeolian bounding surfaces (reactivation, superimposition surfaces). Grainflow deposits and wind ripple lamination	Kocurek (1996), Scherer (2000), Mountney (2006a, 2006b),
Low-angle aeolian deposit LA-A	Fine-grained to coarse-grained sandstones and granules. Laterally extensive sand bodies, layers dipping ≤15°.	Subcritically climbing translatent strata, wind ripples. Interbedded dipping fine-grained and coarse-grained to granule layers. Granule pavements, granule linings	Kocurek (1986), Clemmensen and Abrahamsen (1983), Fryberger et al. (1992), Maxwell and Haynes (2001).
Aeolian sandsheet ASS	Flat-horizontal, tabular bodies formed by fine-grained yellowish sandstone organized in tabular m-thick intervals.	Subcritically climbing translatent strata, granule ripples, adhesion ripples, granule pavements, pin-stripe lamination. Root traces	Hunter (1977), Kocurek and Fielder (1982), Clemmensen and Abrahamsen (1983), Fryberger et al. (1983).
Damp interdune DI	Dark yellow to brown medium- to coarse-grained sandstones. Related with wet interdune and aeolian dune facies.	Wavy and disrupted lamination.	Mountney and Thompson (2002), Rodríguez-López et al. (2008).
Wet interdune WI	Sandy mudstones and siltstones. Tabular meter-thick intervals merging laterally with aeolian dune toe-sets.	Massive, laterally continuous lamination.	Mountney and Thompson (2002), Stanistreet and Stollhofen (2002).
Alluvial system			
Debris flow DF	Tabular intervals of pebble-boulder, clast- to matrix-supported disorganized to poorly organized conglomerates. Sharp-flat to slightly erosive bases. Sandy tabular intervals with floating pebbles and cobbles.	Generally massive and disorganized; locally crude lamination, inverse grading; large protruding boulders at the top. Locally crudely imbricated clasts and parallel alignment of clasts. Vertically oriented clasts.	Nemec and Steel (1984), Chamyal et al. (1997), Enos (1977), Sohn (2000).
Cobble-sand sheetflood CS-SS	Conglomerates with slightly erosive bases. Tabular and laterally continuous intervals.	Internal crude cross-bedding	Turner (1980).
Sand-silt sheetflood SS-SF	Tabular meter- to decimeter-thick intervals of muddy sandstones and siltstones.	Structureless, mottling.	Collinson (1996), Jo et al. (1997).
Boulder to sand bedload stream BS-BS	m-thick lenticular clast-supported channelized conglomerates. Massive conglomerates infilling ribbon-like channels with overhanging walls. Matrix of pebbly sand. Superimposed concave-up surfaces.	Medium-scale cross-bedding. Foresets dip near 23°. Large-scale planar cross-bedding sets with dips near 11°.	Ramos and Sopeña (1983), Chamyal et al. (1997), Jo et al. (1997), Bhiry and Occhietti (2004).
Pebbly sand bedload stream deposit PS-SB	Fine- to medium-grained sandstones with basal cobble lags. Lower sharp and erosive bases with vertical walls. Gravel pockets.	Crude horizontal lamination, planar to tangential cross-bedded sets.	Jo et al. (1997), Blair (1999)
Intraformational conglomerate channel fill IC	Sub-rounded to sub-angular finely laminated sandstone blocks forming disorganized conglomerates infilling ribbon-like channeled bases. Sandy matrix and floating extraformational pebbles.	No specific orientation of sandstone blocks	Deynoux et al. (1989) Mountney and Howell (2000)

Thompson, 2002). This facies is spatially related and merged laterally to the aeolian dune sands and to the clays of the interdunes (see Rodríguez-López et al., 2008) indicating that the phreatic level was high and intersecting the depositional surface while dune advanced creating a climbing wet aeolian system. The aeolian deposition system also contains fine-grained (muddy) sediments accumulated in wet interdunes depressions. Rodríguez-López et al. (2012a) reported the inter-tonguing of dune toe-set deposits with interdune strata reflecting aeolian dune advance contemporarily with interdune sedimentation (e.g. Gradziński and Jerzykiewicz, 1974; Stanistreet and Stollhofen, 2002).

3.2. Alluvial depositional system

The El Pobo Range delivered carbonate clasts through alluvial fans and associated distal fluvial systems that interacted with encroaching aeolian dune fields in the Teruel Basin (Rodríguez-López et al., 2012a). The alluvial depositional system displays typical facies associations related with alluvial dynamic in such environments including proximal to middle and distal fan facies associations (Table 1): debris flow (DF) deposits, cobble-sand sheet flood (CS-SF), boulder to sand bedload stream deposits (BS-BS), pebbly sand bedload stream deposits (PS-BS), and sand-silt sheet floods (SS-SF). Debris flow deposits display pebble-boulder, clast- to matrix-supported, disorganized to poorly organized conglomerates with sharp-flat base with inverse grading indicating a basal shear zone during deposition (Rodríguez-López et al., 2012a; cf. Nemec and Steel, 1984). Cobble-sand sheetflood deposits are organized in tabular and laterally continuous levels of conglomerates with crude cross-bedding with sharp-flat top surfaces locally covered by deflation lags. Boulder to sand bedload stream deposits consist of clast-supported channelized conglomerates forming meter-thick lenticular bodies with deeply sharp and erosive bases sometimes showing vertical to overhanging ribbon-like channel walls. Pebbly sand bedload stream deposits consist of fine- to coarse-grained sandstones with basal cobble lags, scattered floating pebbles, and pebble pockets, showing crude lamination and planar and tangential cross-bedded sets (Rodríguez-López et al., 2012a; cf. Blair, 1999). Sand-silt sheetflood deposits are formed by muddy sandstones and siltstones organized in structureless tabular, decimeter- to meter-thick levels. They are interbedded with stream-flow conglomerates and show mottling and well-defined red and brown horizons (cf. Collinson, 1996; Jo et al., 1997).

During flood events, the water flows coming from the alluvial fans interacted and cross-throughout the aeolian dune field leading to intense erosion and reworking of aeolian sands forming intraformational sandstone-conglomerate channel fills (cf. Mountney and Howell, 2000; Deynoux et al., 1989; Rodríguez-López et al., 2012b). This facies association is formed by sub-rounded to sub-angular, cobble to boulder size (9–57 cm) sandstone intraclasts filling ribbon-like channel incisions in aeolian sandsheet deposits. Aeolian intraclasts are mixed with carbonate extraformational pebbles as those contained in the alluvial facies, indicating that the flows that cross through the aeolian dunefield come from the nearby highlands of the El Pobo Range.

4. Soft-sediment deformation structures

4.1. Studied outcrops

Walls of two quarries have been investigated in order to recognize and study soft-sediment deformation structures and to analyze the relationships between SSDS geometry and the sedimentary facies in which they developed. These quarries are referred here as South Quarry (SQ) and North Quarry (NQ) and are located at distances of 2.0 and 1.7 km, respectively, from the main active Sierra del Pobo fault trace (see location in Fig. 1C). Usually, the quarry walls make available high-quality, and relative continuous (>30 m) outcrops, although their lower parts are progressively covered by fallen debris due to wall degradation.

The South Quarry is discontinuously used for extracting aeolian sands as material for construction. The successive quarry walls offer good exposures where the sedimentary facies and their lateral and vertical relationships or the SSDS affecting them can be observed (Fig. 2). One previous wall of the SQ was studied by Lafuente et al. (2008) and Rodríguez-López et al. (2012a), who described different local SSDS ascribed to seismic and animal tracking. The results presented here included the observations made in this quarry in two field campaigns (July 2011 and November 2015). A part of this quarry wall displayed in November 2015 is shown in Fig. 2, which shows the main facies associations recognized during field survey and their lateral and vertical relationships. Six continuous deformed beds (levels 1–6) and other isolated SSDS have been recognized (see location in Fig. 2).

The North Quarry remains inactive, at least, from the year 2000. The outcropping local stratigraphical series comprises a lower part consisting of yellow and white sands and silts and a level of red clayed silt and an upper part mainly consisting of carbonate breccias and conglomerates belonging to the *Villafranchian pediment* unit (Fig. 3). In this quarry wall, a discrete deformed level has been observed (see location in Fig. 3).

4.2. Deformed beds and involved facies associations

The six deformed beds in the South Quarry (see location in Fig. 2) affect both aeolian and alluvial facies. The three lower deformed beds (named 1, 2 and 3 in Fig. 2) are composed of an alternation of sand laminae of different grain size, from fine to coarse, with fine intercalations of muddy silts. Sandy facies mainly corresponds to aeolian sandsheet (ASS) and low-angle aeolian (LA-A) deposits, and the silts to wet interdune (WI) deposits (Table 1).

Deformed beds 1 and 2 have a lateral continuity of about 8–10 m and a thickness of 10–15 cm, while deformed bed 3 is 25–30 cm thick over a lateral continuity of >25 m (Figs. 2 and 4). Animal tracks affecting these aeolian sandstones have been also observed. Similarly, animal tracks affecting aeolian sandsheet and dune deposits in a previous wall of this

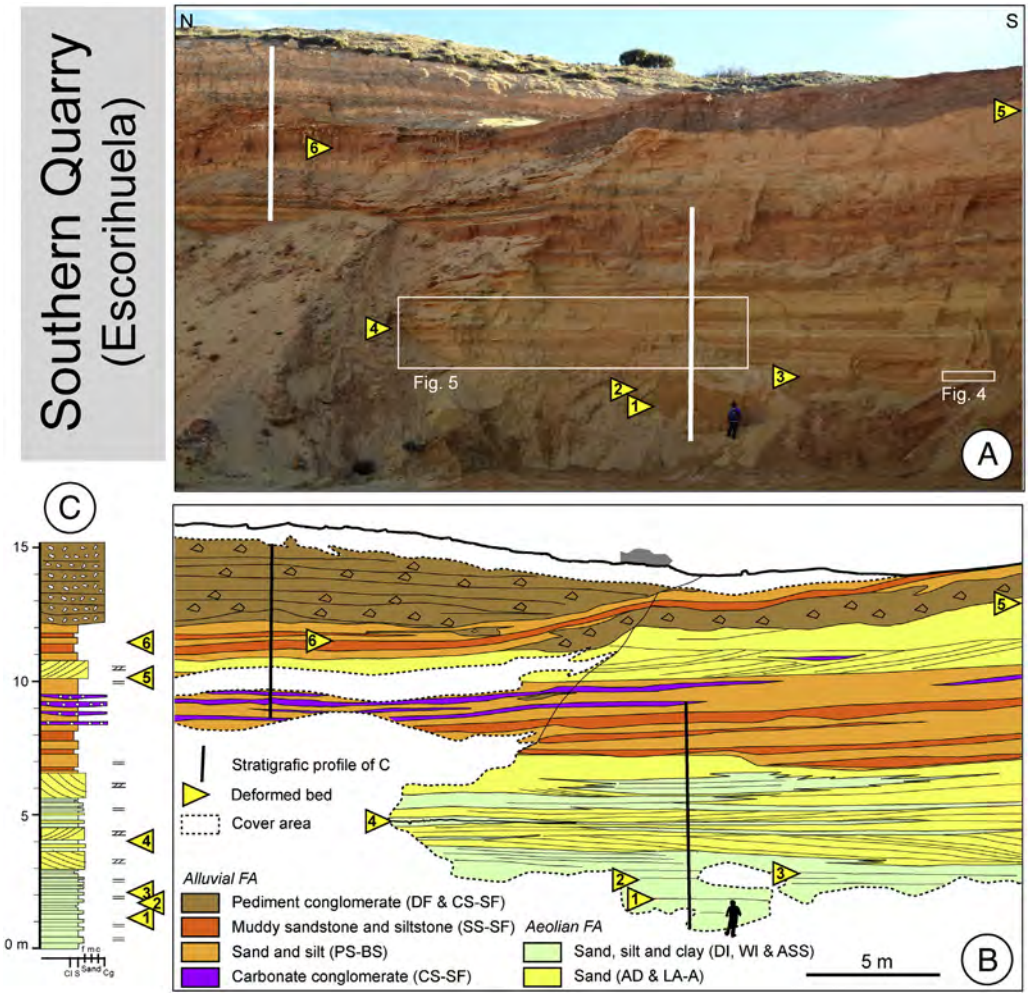

Fig. 2. (A) Photograph of the Late Pliocene aeolian yellow sandstones and the uppermost Villafranchian pediment conglomerates at the Escorihuela South Quarry (see location in Fig. 1C) and the location of the six studied deformed beds. (B) Line drawing on (A) showing the main alluvial and aeolian facies associations distinguished and their stratigraphical architecture. (C) Composite stratigraphic log (white lines in A) with the location of deformed beds.

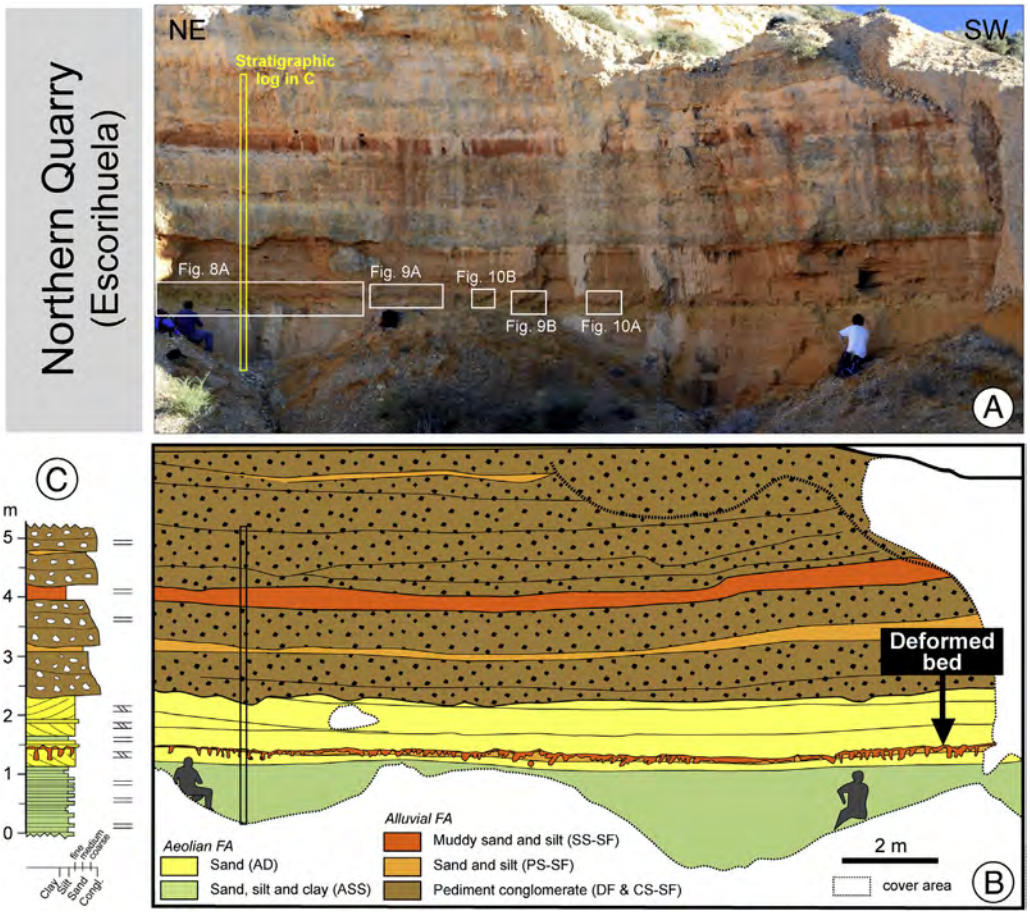

Fig. 3. (A) Photograph showing the southern part of the wall of the Escorihuela North Quarry (see location in Fig. 1C) and the location of deformed bed. (B) Line drawing on (A) showing the main alluvial and aeolian facies associations distinguished and their stratigraphical architecture. (C) Stratigraphic log (white line in A) with the location of the deformed bed.

quarry have been described in detail and interpreted by Rodríguez-López et al. (2012a, their Figs. 10 and 11). These authors show that the animal tracks appear located and concentrated at discrete intervals or locally stacked vertically (but always in different discrete levels), and always covered by non-deformed, flat-lying aeolian deposits (Fig. 4D and E). They distinguished between simple structures (Fig. 4D) from other bilobate structures (Fig. 4E) that they attributed to different animals. Both types of structures show common features in cross-sections such us general concave-up geometry defined by deformed pin-stripe lamination, folded lamination, vertical walls, two marginal upfolds, the concavity of the structures dying out at a discrete level (Rodríguez-López et al., 2012a). These structures appear filled with a variety of sedimentary facies including floating granules and massive texture, laminated sands arranged in cm-thick lamina preserving pin-stripe lamination, a chaotic infill with parts cemented by carbonates, or locally brecciated pin-stripe lamination.

In the three deformed beds (1–3) of the South Quarry, load structures and some associated fluid-escape structures have been identified in addition to animal tracks. These deformed beds show gentle deformation of the laminae, with small load casts (10–20 cm wide) and some dish and pillar structures (Fig. 4). Load casts are developed in sandy layers with slight differences in grain size. Dish and pillar structures develop when fine laminae of silt are intercalated in sandy sediments. In these three deformed beds, SSDS are spaced 0.3–1 m.

Higher in the stratigraphic record, a ~15-cm-thick, deformed bed is observed over 6 m of lateral continuity (bed 4). Deformation is well constrained to the presence of interdune facies (both damp and wet interdune facies) encased in through cross-bedding dune sandstones (Fig. 5). Soft-sediment deformation structures, mainly small drop structures (<5 cm wide and 5–15 cm long; Fig. 6), are developed in three units composed, from bottom to top, of fine to medium sand (damp interdune facies), grey clayey silt (wet interdune FA), and overlaying sand (aeolian dune apron facies). These aeolian dune aprons are characterized by bimodal deposits consisting of granules and fine-grained sands organized in coarser grainflow wedges pinching out upwards into finely laminated aeolian dune foresets, and downwards into wind ripple-laminated sands (see Rodríguez-López et al., 2012a).

At the top of the Escorihuela Formation, located 1–2 m below the sharp contact with the overlying Villafranchian pediment gravels, two deformed beds are located in the alluvial facies. Bed 5 crops out 20 m out of the photograph of Fig. 2 and it was walked for a distance of 3 m, because it was truncated southwards by overlying channeled and gravely bedload stream deposits (facies BS-BS) (Fig. 7A). Bed 6 was investigated in the quarry wall during the July 2011 campaign and its stratigraphic location is situated in the photograph. This level was continuous in the observable outcrop (>6 m) and involved sedimentary facies and SSDS morphologies and dimensions (Fig 7B) were similar to level 5 (Fig. 7A). Thus, two units constituted both deformed beds: coarse sand and dispersed pebbles (cobble-sand sheet floods) overlying medium to fine sand (sand-silt sheet floods). Sagging and irregular load casts (sensu Anketell et al., 1970; Alfaro et al., 1997, 1999) characterize these deformed beds. Lamination and stratification of the upper deformed bed are perfectly continuous and have a convex downward morphology. Between two convex lobes, the lamination and/or stratification forms an acute upward-directed angle (Fig. 7). The size of these structures varies between 20 and 40 cm in width and 15–20 cm in height. In both cases, the deformation was fossilized by a deflation lag characterized by laterally continuous accumulation of pebbles scattered

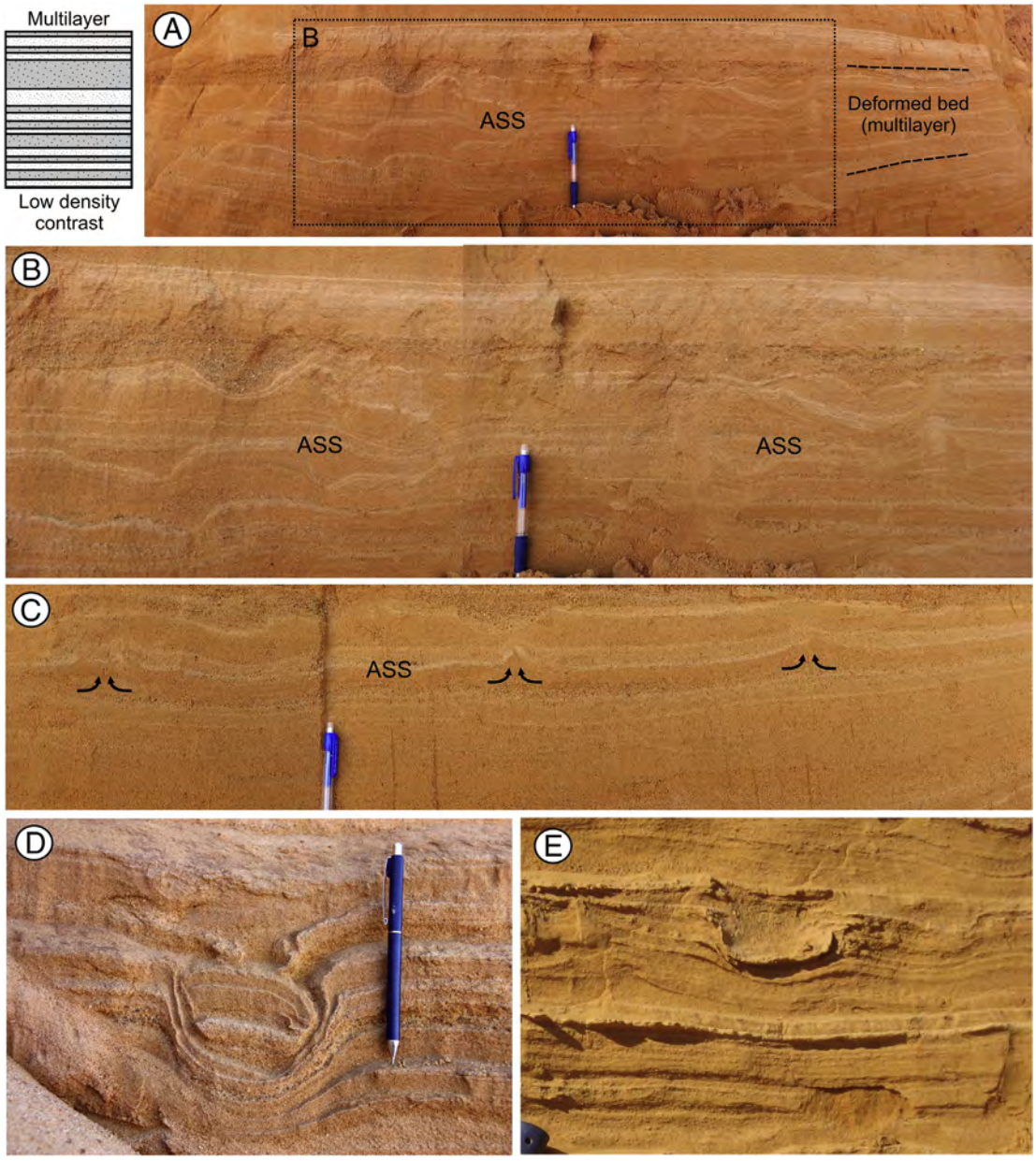

Fig. 4. (A) Panoramic view of the deformed bed 3 (South Quarry) characterized by a multilayer of medium- to fine-grained sands of aeolian sandsheet (ASS) (see location in Fig. 2A). (B) Detailed view of structures (see A for location) with slight deformation, characterized with load structures with large lateral spacing (from 30 cm to 1 m). (C) Fluid-escape structures, such as dish and pillars, are related to the presence of thin barriers of permeability. (D) and (E) SSDS with simple or bilobate geometry, respectively, associated to animal tracks.

through the surface and sharply covered by flat-laying and laminated yellow medium- to coarse-grained sands corresponding to aeolian dune (AD) deposits. Deflation of sheet floods in aeolian dune fields generates these kinds of architectures in the sedimentary record (see Rodríguez-López et al., 2010). This deflation lag postdates deformation and formed just before a renewal period of dune migration and accumulation.

A very well-exposed deformed horizon is observed in the North Quarry (Fig. 3). This deformed horizon is continuous and extends laterally for 20 m, allowing the observation of structures both in cross-section (Fig. 8) and plan view (Fig. 9A). The SSDS can morphologically be described as load casts, drop structures, and pillows (sensu Anketell et al., 1970; Alfaro et al., 1997; Owen, 2003). Differential erosion offers some small outcrops in plan view where elliptical and circular morphologies of load structures are observed (Fig. 9A), similar to those previously described in literature (e.g., Gibert et al., 2011). Locally, only in 1.5 m of extent of the deformed bed, vergent load structures are present (Fig. 10). The deformed bed (10–25 cm in thickness) is composed of four lithological units from bottom to top (sector 1 in Fig. 8): (i) unit A—fine-grained yellow sands (aeolian dune or sandsheet deposit), (ii) unit B—medium- to coarse-grained sands (pebble-sand bedload stream deposit), (iii) unit C—silt with dispersed sand grains (SS-SF and CS-SF facies), and (iv) unit D—medium- to coarse-grained sands (aeolian dune facies association). A relevant feature of this deformed bed is that laterally, in a ~2-m-wide zone (sector 2 in Fig. 8), deformation is limited to units B, C, and D, while unit A looks undeformed. In sector 2, the morphology of SSDS is similar to sector 1, albeit smaller because their confinement to a thinner bed.

5. Discussion

In this chapter, the mechanisms of deformation and driving force, as well as the trigger mechanisms of the studied SSDS are discussed. After that, the control of the sedimentary facies on the development, areal

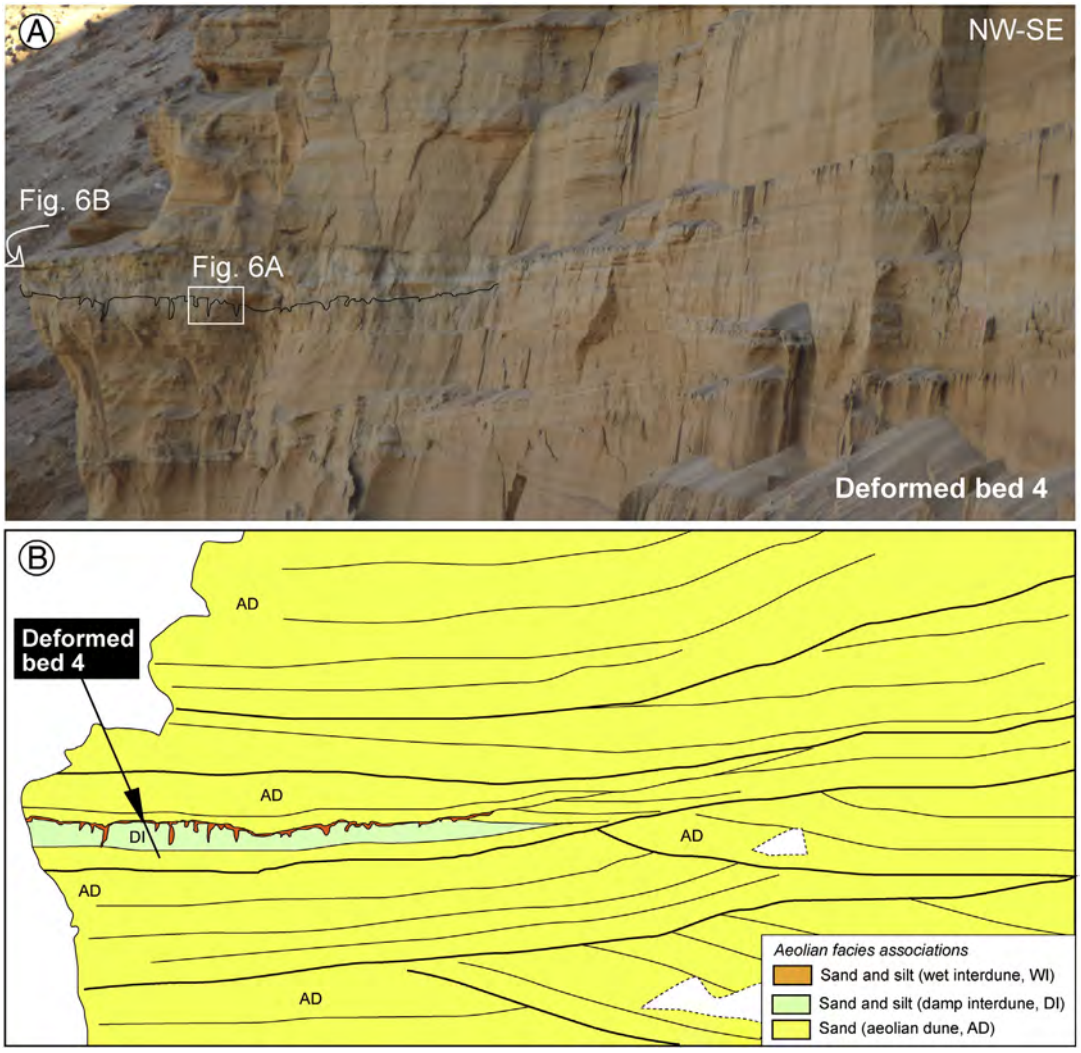

Fig. 5. (A) Panoramic view of the deformed bed 4 (load structures are highlighted) in the South Quarry (see location in Fig. 2A). Location of Fig. 6A and B are included. (B) Line drawing of Fig. 5A showing the involved facies associations and their stratigraphic architecture. Note as the soft-sediment deformations structures (mainly drop structures) are especially displayed by the grey silts of wet interdune (WI) deposits and they disappear when this facies pinches out southwards and only aeolian dune (AD) sands are present.

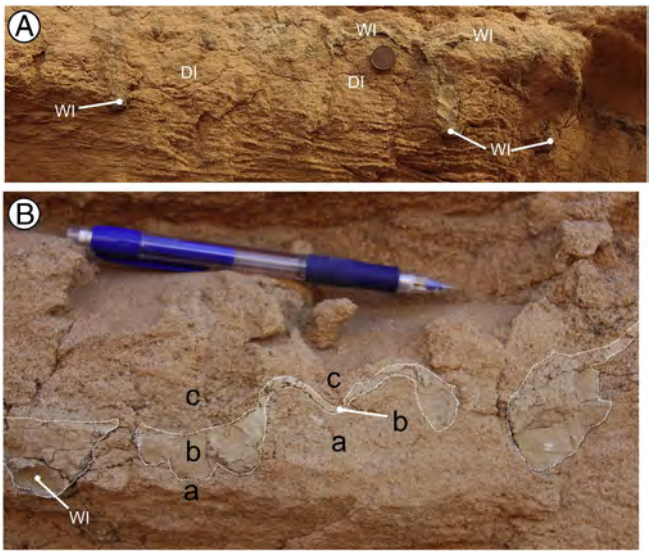

Fig. 6. Details of the SSDS of deformed bed 4. (A) Wet interdune (WI) facies sinking into damp interdune (DI) facies and depicting drop structures. (B) Detail of the three sedimentary units (a, b, and c) involved during deformation (see text for explanation). See Fig. 5A for location of Figs. 6A and 6B.

distribution and geometry of soft-sediment deformation structures is considered and analyzed. Finally, the significance of these seismically induced SSDS is discussed in terms of palaeoseismicity. In particular, we try to estimate the magnitude of the causative earthquakes and the number of seismic events recorded in the depositional system.

5.1. The driving force: Variability of density gradient systems

The studied SSDS were produced by liquefaction of cohesionless sediments, when their strength was temporarily reduced (sensu Allen, 1982; Owen, 1987). The sediment behaved like a viscous fluid or a plastic solid of reduced yield strength (sensu Allen, 1982; Owen, 1987). In the particular case of water-escape structures, fluidization was necessary (sensu Lowe, 1975).

After analyzing different possible driving forces including gravity acting on slopes, unequal loading, gravitational instabilities due to a reversed density gradient, shear by aqueous or other currents, and biological and chemical agents, we consider the reversed density gradient (sensu Anketell et al., 1970) as the main driving force of all deformed beds based on the initial characteristics of the system in the study area. Although the bulk density of involved sediments has not been determined (the present-day values are surely different from those during deformation), coarse-grained siliciclastic sediments are generally denser than fine-grained ones (e.g., Anketell et al., 1970; Allen, 1982,

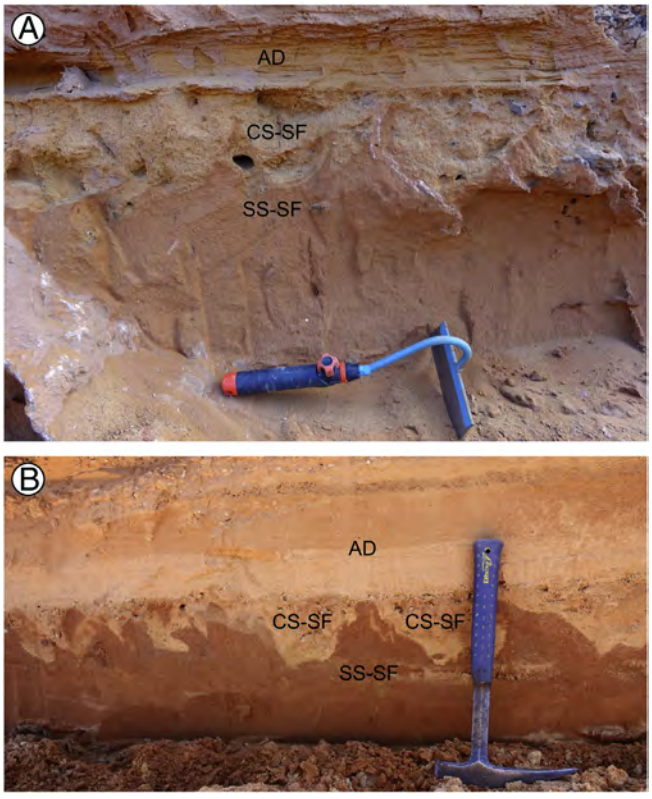

Fig. 7. Sagging and irregular load casts of the deformed beds 5 (A) and 6 (B) in the South Quarry (see Fig. 2 for location). In both cases, deformed deposits include cobbles and sand (CS-SF facies), above, and sand and silt (SS-SF) associated to sheet flood events. Soft-sediment deformation structures are covered by aeolian dune (AD) deposits.

Fig. 9.9). Denser sediment overlies less dense sediment in the studied deformed beds; for instance, in beds 5 and 6 (Figs. 2 and 7), a denser unit (coarse sand and dispersed pebbles) of cobble-sand sheet flood deposits sunk into a less dense sedimentary unit (medium to fine sand of sand-silt sheet flood deposits). Deformation is driven by the gravitational forces associated with the reversed density system and is dominated by vertical displacements (Fig. 7). Deformed bed 4 is another example of the necessity of a driving force (e.g. a reversed density gradient system) to produce deformation during liquefaction. These deformed interdune facies (Fig. 5) merged laterally to homogeneous aeolian sands, where apparent deformation disappears (aeolian sand below and above the stratigraphic contact). Deformation recorded in these simple reversed density gradient systems (e.g. deformed beds 5 and 6 in the South Quarry) are pervasive in our sedimentary succession.

On the contrary, the deformed bed 4 of South Quarry and the deformed bed of North Quarry represent complex reversed density gradient systems, where the upper denser layer is composed of several sedimentary units of different lithology and rheology. In bed 4 (Fig. 6), the denser layer is composed of two units; the wet interdune grey clayey silts (unit b), below, and the aeolian dune medium- to coarse-grained sands (unit c), above, both overlying a unit of damp interdune facies formed by silty medium-grained sands (unit a). In this case, the upper denser layer (aeolian dune) drag and sunk the underlying wet interdune silty facies, constituting together a set with higher density over the underlying damp interdune silty sands (unit a), resulting in a set of well developed drop structures.

In the deformed bed of the North Quarry (Fig. 8), the units B (PS-BS facies), C (mainly SS-SF facies), and D (AD facies) constitute an upper set of relatively higher density than unit A (AD facies). This bed offers a curious lateral variation of the reversed density gradient system (see sector 2 in Fig. 8). In this sector, unit A becomes undeformed, unit B is thicker and constitutes the lower part (less dense) of the system, and the upper part (denser) is constituted only by units C and D. As previously mentioned, types of SSDS (drop and pillow structures) are similar in both sectors, only varying the size of structures. This is probably due to the lower contrast in density of the involved sedimentary facies in sector 2 (Fig. 8). A similar case was described by Owen and Moretti (2008) in Upper Carboniferous delta deposits of south-west Wales.

Both deformed beds with complex reversed density gradient systems have a unit of finer (less dense) sediment (silt and silty clay units) in the upper denser layer. In both cases, these silty units act as a secondary layer, as a part of a denser set with other units of coarser grain size. The silty units act as a passive layer and collapse together with the coarse sand unit into the underlying finer sand layer.

Other relevant feature of the studied stratigraphic succession is the difference in style of deformation among beds. The slight deformation (gentle load cast and low pillar and dish structures) of the deformed beds 1, 2, and 3 (Fig. 4) is related to a low contrast of density in the reversed density gradient system, which is characterized by thin sandy units with slight differences in grain size related to aeolian sandsheet (ASS) deposits and, laterally, to low-angle aeolian (LA-A) deposits. The low contrast in density is probably the cause of the great spacing (0.3–1 m) between these individual SSDS. In these deformed beds, dish and pillar structures are developed where thin silt layers act as barriers of permeability. In this particular case, deformation is formed when sediment is transported by the expulsion of pore water (sensu Lowe, 1975), related to shear by aqueous.

Finally, vergent load structures are only observed in a small part (walked through a distance of 2 m) of the deformed bed studied in the North Quarry. Therefore, gravity acting on slopes can be invoked as an additional driving force in this particular sector of the deformed bed. Albeit, the contribution of unequal loading cannot be discarded, since it is expectable in an environment dominated by migrating dunes, and it can locally increase the magnitude of load structures (e.g. Horowitz, 1982; Bryant et al., 2013).

5.2. Triggers of the studied soft-sediment deformation structures

Many natural agents and process can act as triggers of deformation, including waves, floods, rapid sedimentation, groundwater movements, and earthquakes, among others (see Owen and Moretti, 2011). Unfortunately, there is not a simple relationship between the type of soft-sediment deformation structure and the triggering agent (Owen et al., 2011). We apply the three-stage approach to trigger recognition by Owen et al. (2011), combining the assessment of facies, potential triggers, and available criteria.

After the detailed facies analysis of alluvial and aeolian facies, both sedimentary (flood, rapid sedimentation) and seismic processes have been identified as potential triggers causing the studied SSDS. Some isolated load structures appearing in coarse gravels above fine sands, with no lateral continuity, are exclusively located in water-related facies of the study area. Probably, they result from overloading during rapid sedimentation (e.g. Rodríguez-López et al., 2010), although they are outside of the focus of this paper. By the same token, some biologically induced SSDS mainly present in sandsheet aeolian facies, which were interpreted as animal tracks by Rodríguez-López et al. (2012a), are also discarded in this study.

The rest of observed SSDS, which are the subject of our study, are grouped into a number of deformed beds within the sedimentary succession, and overlied by non-deformed and flat-lying facies with undisturbed lamination (see Figs. 4 and 7), thus excluding overloading as a trigger mechanism. The combination of the following criteria points to the hypothesis of earthquakes as trigger mechanisms for these deformed beds: a) the SSDS are not isolated, appearing in laterally continuous beds separated by undeformed sediment; b) within each deformed bed, individual SSDS exhibit regular spacing, suggesting a synchronous and instantaneous origin for the structures (Oliveira

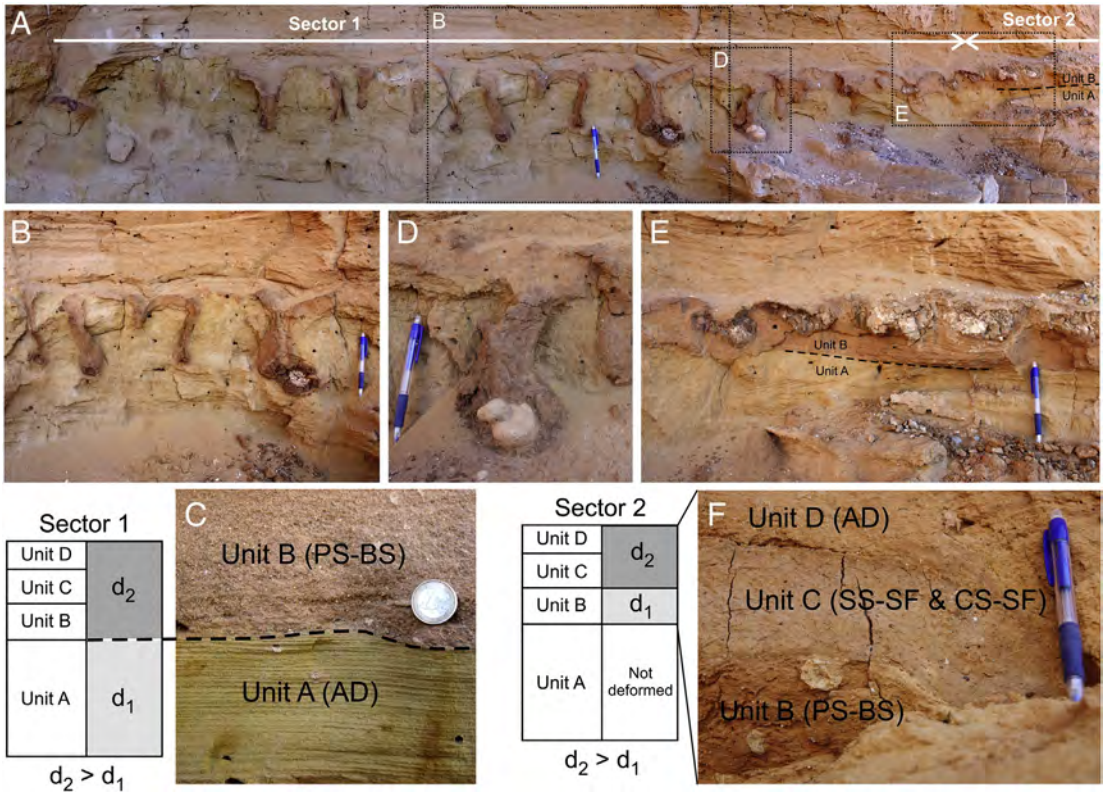

Fig. 8. Features of the deformed bed recognized at the North Quarry. (A) Photograph showing a part of the deformed bed recognized (see location in Fig. 3A) with load structures (mainly drop structures and some pillows). (B) and (C) Details of sector 1 showing how the aeolian dune sands (unit A) is the underlying layer of the reversed density gradient system (d_1, d_2: density). (D) Detail of a drop structure with a carbonate nodule in its nucleus. (E) and (F) Details of sector 2 (see location in Fig. 8A) where unit A shows no apparent deformation and unit B (pebble-sand bedload stream facies, PS-BS) is the underlying layer of the reversed density gradient system; pillows become the main deformation structure. Photographs of C) and F) are located outside the general photograph of A).

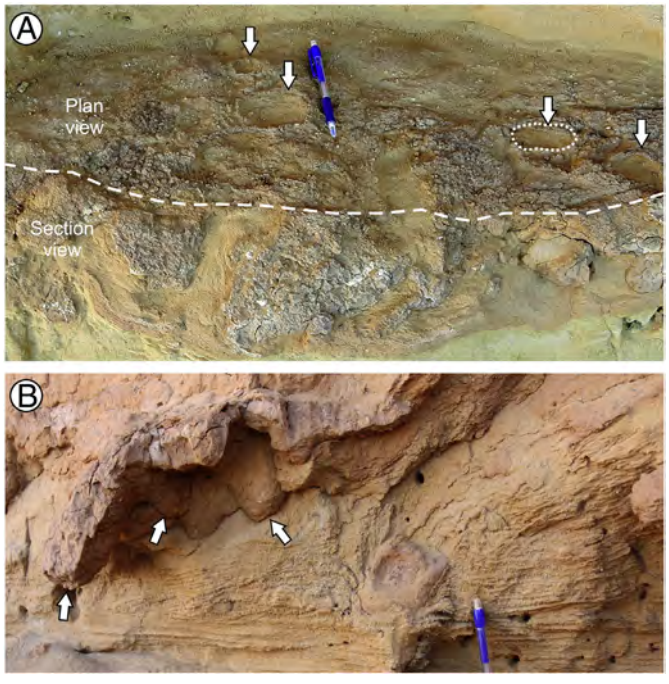

Fig. 9. 3D view of structures of the North Quarry deformed bed (see location in Fig. 3). (A) White dashed line separate section view (lower part of the photograph) and plan view (the upper part) of structures. White arrows point to the elliptical shape in plan view of these load structures. A dot white line marks one of these elliptical structures. (B) 3D view of the base of one of the deformed levels. White arrows point to the lobate morphology of load structures.

et al., 2009); c) the studied SSDS are located in a tectonically active basin during the Late Pliocene, 2 km from the Sierra del Pobo active fault zone, and at a distance of <50 km from other active normal faults (Concud, Sierra de Palomera, or Teruel faults; see location in Fig. 1B) (e.g., Gutiérrez et al., 2008, 2012; Lafuente et al., 2011; Liesa, 2011; Simón et al., 2012); d) in an ancient wall of the South Quarry, Lafuente et al. (2008) described and interpreted numerous cases of seismically induced SSDS, some of them controlled by either the local prevailing fracture set or the maximum horizontal stress (S_{Hmax}), therefore linking them to tectonic activity; and e) similar load structures have been described in recent earthquakes (e.g., Sims, 1975; Thakkar and Goyal, 2004).

5.3. Facies control on the development of seismites

Lateral extent of deformed levels was considered by Sims (1975) and other authors (e.g., Obermeier et al., 1990; Hilbert-Wolf et al., 2009; Owen and Moretti, 2011) as a diagnostic criterion of seismically induced SSDS. This criterion is based on the threshold necessary for seismically induced liquefaction, which results in liquefaction affecting large areas (even >100 km from the epicenter for high-magnitude earthquakes, Obermeier, 1996; Galli, 2000). However, as previously indicated, sedimentary facies exert a main control on the development of seismites in most sedimentary environments (Moretti and van Loon, 2014, and references therein). Therefore, the actual extent of the deformed beds can be significantly smaller than the potential one. First, vertical facies changes due to authigenic sedimentary processes provide the reversed density gradient necessary for bed deformation by gravitational forces after seismic instability, while bed thickness can control the size of SSDS (Alfaro et al., 2010). Second, lateral facies changes strictly determine the areal extension of the overall seismic liquefaction effects, so the continuity of individual deformed beds is largely

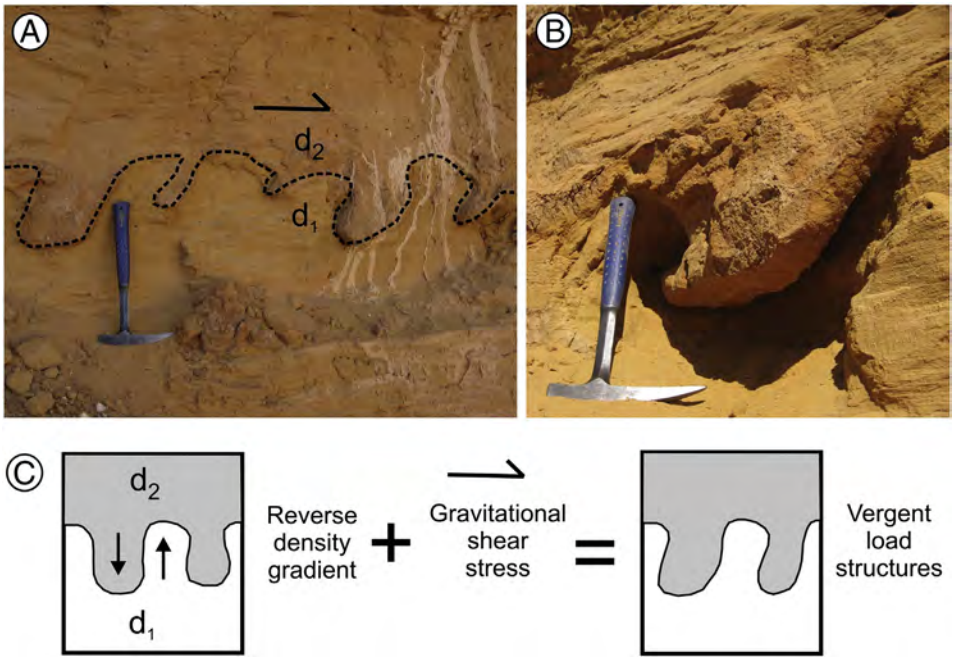

Fig. 10. (A) and (B) Vergent load structures in a sector of the North Quarry deformed bed (see location in Fig. 3). (C) Local gravitational shear stress produces asymmetric load structures (sketch modified from Moretti et al., 2001).

controlled by the own lateral continuity of sedimentary environments (e.g., Rodríguez-López et al., 2007; Alfaro et al., 2010; Moretti and van Loon, 2014; Ezquerro et al., 2015, 2016).

The development and areal extent of the studied deformed beds in the Pliocene Escorihuela dunefield seems to be clearly controlled by vertical stacking and lateral changes of the alluvial and aeolian sedimentary facies. SSDS are mainly developed in specific successions of alluvial and aeolian sedimentary facies, namely those including saturated sediments (necessary for liquefaction to occur) composed of interbedded gravel, sand, and silt (which provide the reversed density gradient).

Among the alluvial facies, the most favorable ones for seismic liquefaction are cobble-sand sheetflood (CS-SF) deposits laying on sand-silt sheetflood (SS-SF) facies, as occur in beds 5 and 6 all along their exposure in the South Quarry wall (Fig. 7). Stacking of these saturated facies enables the reversed density gradient, which favors deformation. The flat-lying attitude and lateral extent of sheetflood deposits, which should be present along the entire active fault scarp, suggest that seismites could have indeed a large distribution along the basin. However, the limited outcrop conditions of the studied sediments prevent to confirm this hypothesis. It is interesting to note that both seismites were preserved by the superposition of aeolian dune deposits, which could increase their potential of preservation.

In the alluvial–aeolian interacting facies, seismites seem to be mainly associated to dunefields affected by flood events, as it occurs in the deformed bed described in the North Quarry. The conceptual model at Fig. 11 shows this situation. Nevertheless, flood by itself should be ruled out as the trigger for studied deformation. In this locality, Rodríguez-López et al. (2012a) described erosional surfaces developed above non-deformed aeolian sediments with an early slight cementation, as evidenced by the presence of intraclasts (blocks) in wadi channel facies (see pre-seismic stratigraphic architecture in Fig. 11). This demonstrates that these high-energy floods were not able to deform previously cemented underlying sediments.

Indeed, in the North Quarry bed, deformation did not occur while the first flood event, but independently and after the flood events. There, the reversed density gradient was determined by the superposition of coarse- to fine-grained sands of aeolian dunes (AD), low-angle aeolian (LA-A) or sandsheet (AS) deposits (unit D) over muddy and silty sands of sheet flood deposits (unit C), which are, as well, lying on previous aeolian fine-grained sands (units A and B). In such a context, when a near earthquake occurred the non-cohesive, lowermost aeolian sediments liquefied and enabled ductile deformation of upper cohesive muddy and silty sheetflood deposits, developing drop and, locally, ball-and-pillow structures (see post-seismic stratigraphic architecture in Fig. 11). This deformed bed laterally correlates (30 m northwards) with the level with cm-scale SSDS (mainly load casts and pillow structures) described by Lafuente et al. (2008), which corresponds to thinner-bedded (cm-scale) flat-lying sandsheet and damp interdune deposits. This lateral change in the involved sedimentary facies is probably responsible for the changing geometry of SSDS along the deformed bed.

Among the aeolian facies, the wet interdune (WI) facies constitutes the most favorable one for seismite development (Fig. 5). Bed 4 in the South Quarry is a good example of the facies control on the development of SSDS in aeolian systems. It is developed in wet interdune (WI) areas and laterally disappears where aeolian dune (AD) facies are involved (Fig. 5). In detail, SSDS developed where different sedimentary facies are vertically stacked, and specifically where they showed a stronger reversed density gradient, i.e., due to a high contrast in grain size. In this case, drop structures developed where the vertical succession of aeolian dune (AD) or sandsheet (ASS), damp interdune (DI), wet interdune (WI), and aeolian dune (AD) facies is recognized, and deformation laterally disappears in a few meters where the uppermost AD facies is directly lying on the basal AD. This constitutes an architectural control on the lateral continuity of seismites as interdune surfaces put in stratigraphic contact the underlying aeolian dunes with the apron deposits of the overlying climbing dune aprons. In this situation, no density gradient exists and no deformation is recorded. This example evidences the strong control of the lateral changes in facies on the areal distribution of SSDS. The conceptual model at Fig. 12 shows the initial pre-seismic stratigraphic architecture of a dunefield affected by a high water table, and its control on seismite development. Seismites only form where the sedimentary succession determined a reversed density gradient, i.e. where fine-grained, wet, and damp interdune deposits are sandwiched between coarser aeolian dune deposits.

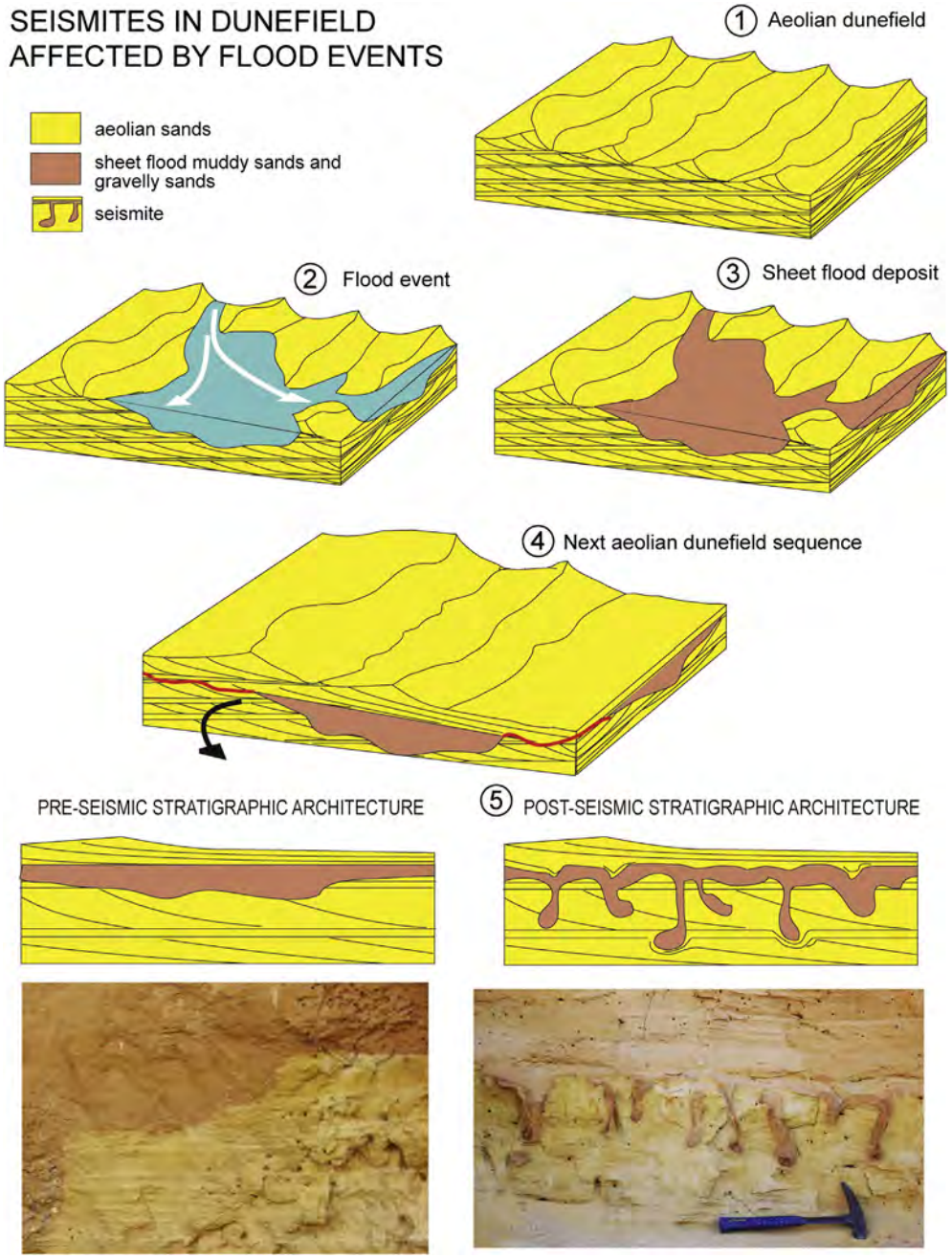

Fig. 11. Conceptual model explaining seismite development in a dunefield affected by flood events. Cartoons 1, 2, 3, and 4 show the succession of sedimentary processes defining the pre-seismic stratigraphic architecture; the left photograph displays that flooding did not produce deformation on basal aeolian sands. Cartoon 5 shows the development of a seismically induced deformed bed in local levels of the stratigraphic succession (right photograph, coming from the North Quarry deformed bed). See text for explanation.

In addition, aeolian sandsheet (ASS) facies are also favorable for seismite development when they are associated to a relatively high water table, as it likely occurred in levels 1, 2, and 3 at South Quarry and in the deformed bed described by Lafuente et al. (2008) at North Quarry. The slight deformation of these beds has been related to the small differences in grain size that show the aeolian sandsheet deposits. It is frequent to find granule linings and coarser layers in these facies associations (see Rodríguez-López et al., 2012a). The reduced thickness (normally <3 cm) of the sand levels with different grain sizes and the flat-lying attitude of this aeolian facies probably are responsible for both the small dimensions of the load structures and their large, although regular lateral spacing. Fluid-escape structures only occur in sectors where silty levels (with slight early cementation) acted as barriers of permeability.

Finally, according to our observations, aeolian sand dunes are less prone for seismite development. Lafuente et al. (2008, fig. 4) described sand dikes in South Quarry probably located within this sedimentary facies. Other SSDS have also been described in the literature (see Moretti, 2000 and references therein). Nevertheless, no clear seismically induced SSDS has been identified in our studied dunes. Usually, dune sands are not saturated, which prevents their liquefaction in spite of their favorable grain size and porosity. However, deformation processes affecting aeolian dunes can occur in desert basins with a fluctuating phreatic level as well as in coastal areas or due to water percolation during rainy periods leading to SSDS in the dune foreset (see Rodríguez-López et al., 2008, and references therein). These kinds of deformation structures have not been recorded in the aeolian sandstones of the Escorihuela dunefield (Rodríguez-López et al., 2012a).

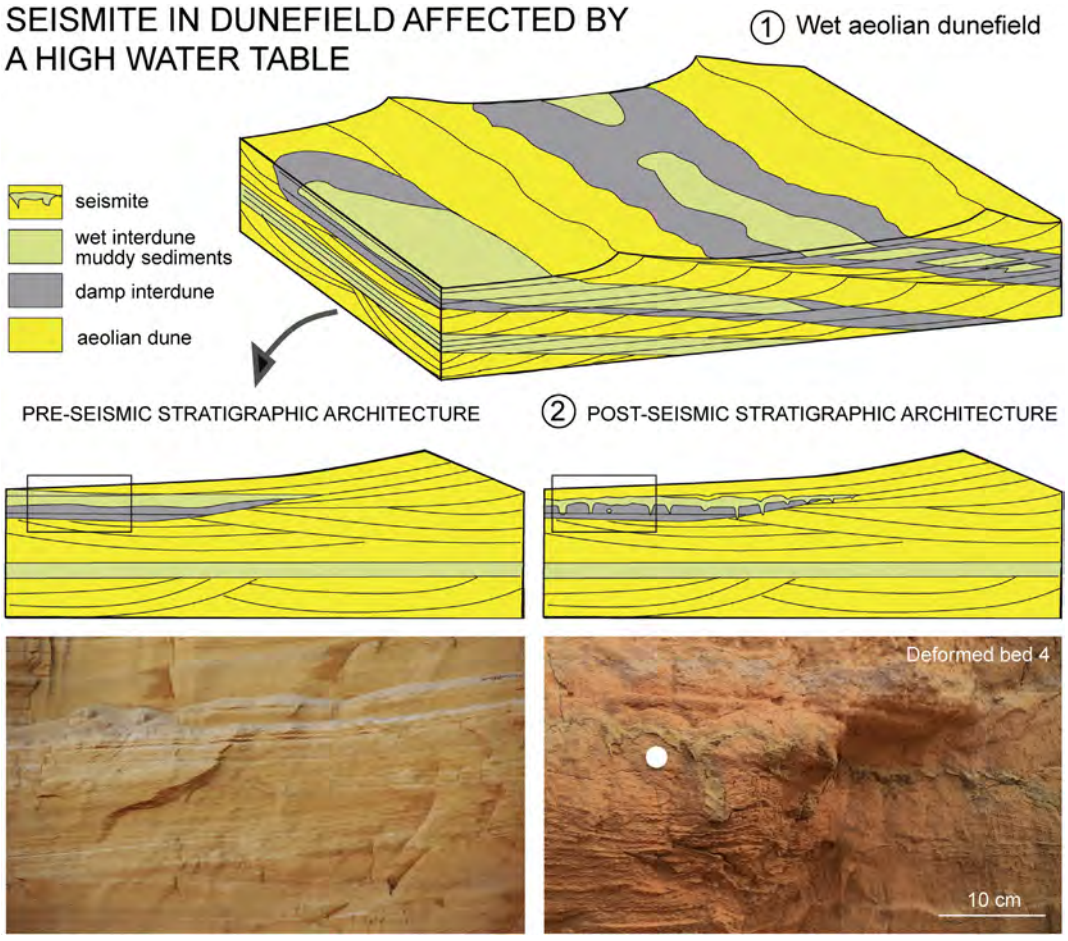

Fig. 12. Conceptual model explaining seismite development in a dunefield affected by a high water table. Pre-seismic stratigraphic architecture shows the limited lateral continuity of wet and damp interdune deposits, and hence the limited extension of the reversed density gradient system that ultimately controls the lateral continuity of the deformed bed. See text for explanation and Fig. 5A for comparison.

5.4. Magnitude of paleoearthquakes

Liquefaction is one of the effects of near-field earthquakes. Several authors (e.g. Atkinson, 1984; Audemard and De Santis, 2001; Papathanassiou et al., 2005) establish Ms = 5.0 as the smallest magnitude that have triggered liquefaction, although there exist some exceptions (Sims and Garvin, 1995, described re-liquefaction during an aftershock of magnitude 4.6 in Loma Prieta, California). Other works evidence that spread liquefaction requires magnitude over 5.5 (e.g., Ambraseys, 1988). Nevertheless, more research is needed for full understanding the relationships between SSDS development and seismic magnitude. Although the size of some SSDS increases with earthquake magnitude (see Obermeier, 1996; Castilla and Audemard, 2007), and the occurrence of some types of seismites could also need exceeding some magnitude threshold (Rodríguez-Pascua et al., 2000), other factors influence size and morphology (Owen et al., 2011). Therefore, we must be cautious when using size or morphology as an indicator of earthquake magnitude (e.g., Alfaro et al., 2010).

Based on the studied stratigraphic sections, we do not have any objective criteria to assign a precise magnitude to the earthquakes responsible of the studied SSDS. We are only able to estimate the most probable interval of magnitude from indirect data. Since the studied outcrops are located some 2 km from an active fault (Sierra del Pobo fault), our interpretation of seismicity as the origin of the studied SSDS is supported by the existence of the needed seismic source. Moreover, as these SSDS were the effect of near-field earthquakes, the minimum magnitude required would have been 5.0. Considering that the Sierra del Pobo fault was able to produce earthquakes up to Mw = 6.8 (see Section 2), we can conclude that the studied SSDS were due to earthquakes with magnitude in the range of 5.0–6.8. We should not discard other possible causative faults in the neighboring region (Concud, Teruel, Palomera, or Calamocha faults; Simón et al., 2012), but this would not change that conclusion since none of them has an associated maximum Mw higher than 6.8 (see QAFI database: IGME, 2012).

Within the stated magnitude range, it is probable that some of our recorded shakes approached its upper limit. This assessment is based on the occurrence of drop and pillow structures, whose degree of deformation probably required long-duration liquefaction, i.e. higher seismic magnitude (Alfaro et al., 1997; Moretti et al., 1999; Owen, 2003).

5.5. Number of recorded paleoearthquakes and recurrence interval

Although alluvial–aeolian interacting deposits may not be as good as lacustrine ones for earthquake recording (e.g., Rodríguez-Pascua et al., 2000; Alfaro et al., 2010; Gibert et al., 2011; Moretti and van Loon, 2014; Ezquerro et al., 2015), they have provided valuable information for improving the knowledge on the tectonic activity of the northern Teruel Basin during Late Pliocene time. Our results show how continental sedimentary systems with high lateral variability in facies can only provide a discontinuous, and probably incomplete, paleoseismic record. Therefore, the reconstructed event succession should be considered as a bare minimum, hence the concept of *apparent recurrence period* (in the sense of Ezquerro et al., 2015) should be applied.

We have identified six deformed beds with irregular distribution in the 15-m-thick succession at South Quarry, and one deformed bed in North Quarry, both in the upper part of the Escorihuela dunefield. Although we have not enough age control, the last deformed bed could be correlated with either bed 5 or bed 6 at South Quarry seeing at their stratigraphic position immediately below the more expansive gravelly deposit of the *Villafranchian pediment* unit (Figs. 2 and 3).

According to the magnetostratigraphical results by Opdyke et al. (1997) and the stratigraphical studies by Ezquerro et al. (2012) and Rodríguez-López et al. (2012a), the age of the studied dunefield sediments ranges from 2.9–2.8 to 2.6 Ma (i.e, spanning ~200–300 ka). If the six identified seismites were associated to activity of the Sierra del Pobo fault, an *apparent recurrence period* about 33–50 ka can be calculated for this fault system. This period is similar to that inferred (45 ka) by Ezquerro et al. (2015) for the Late Pliocene–Early Pleistocene seismic history of the near Concud Fault from the recognition of 21 seismic events (seismites) in palustrine sediments. Nevertheless, taking into account that the vertical slip rate (since 3.6 Ma) of the Sierra del Pobo fault is quite larger than that of the Concud Fault (0.11 vs. 0.07 mm/a), a lower apparent recurrence period was to be expected for the Sierra del Pobo fault. This discrepancy can be likely attributed to a lower efficiency of alluvial–aeolian environments for seismite development when compared with lacustrine ones.

6. Conclusions

Two exceptional exposures have been investigated in a Pliocene dunefield in order to recognize seismically deformed beds and their relationships with alluvial and aeolian sedimentary facies. Both outcrops correspond to quarry walls (North Quarry and South Quarry) located south of Escorihuela, at the northern part of the Teruel half-graben (eastern Iberian Chain). Besides a number of isolated soft-sediment deformation structures, six levels with abundant SSDS were recognized in South Quarry and one level in North Quarry.

In addition to animal tracks, described previously in the studied succession, load structures are the most common SSDS. They are developed in beds made of two or more layers with a reversed density gradient. According to the morphology of the interface between deformed layers, sagging load casts, drop structures casts, and pillows were identified.

The distribution of deformed beds in the stratigraphic succession is irregular, showing a strong relationship with sedimentary facies, especially with water-related facies. Aeolian sands show a lower number of deformation structures, these being mainly developed in wet interdune facies and, locally, aeolian sandsheets. Alternation of sand and silt and their relative thickness control the development and size of deformation structures. In the alluvial system, deformed beds are related to sheet flood deposits. Lateral changes in facies strongly control the areal distribution and geometry of seismites. In summary, development and distribution of seismites are controlled by the lateral and vertical distribution of favorable sedimentary facies, which is ultimately defined by the own dynamics of the sedimentary system and its time evolution.

The deformed beds are interpreted as a result of earthquakes with a magnitude between 5.0 and 6.8. The existence of drop and pillow structures in some deformed beds suggests that the actual magnitude could be closer to upper value. Palaeoearthquakes are probably related to the activity of the near (2 km) Sierra del Pobo normal fault zone. The succession of six deformed levels has allowed us to infer an *apparent recurrence period* of 33–50 ka for the characteristic palaeoearthquake of this fault during the 2.9–2.6 Ma interval, similar to other active faults in central-eastern Iberia.

Acknowledgments

The authors are grateful to Dr. Massimo Moretti and Dr. Carlos Oliveira for detailed reviews and useful comments and suggestions. Research has been financed by projects CGL2012-35662 and CGL2011-30153-C02-02 of Spanish Ministerio de Economía y Competitividad-FEDER, as well as by the Aragón regional government ("Geotransfer" research group).

References

Alcalá, L., Alonso-Zarza, A., Álvarez, M.A., Azanza, B., Calvo, J.P., Cañaveras, J.C., van Dam, J.A., Garcés, M., Krijgsman, W., van der Meulen, A.J., Morales, J., Peláez, P., Pérez-González, A., Sánchez, S., Sancho, R., Sanz, E., 2000. El registro sedimentario y faunístico de las cuencas de Calatayud-Daroca y Teruel. Evolución paleoambiental y paleoclimática durante el Neógeno. Revistas de la Sociedad Geológica de España 13, 323–343.

Alfaro, P., Estévez, A., Moretti, M., Soria, J.M., 1999. Sedimentary deformation structures interpreted as seismites in the Quaternary of the Low Segura basin (Eastern Betic Cordillera). Comptes Rendues de l'Academie de Sciences de Paris (II) 328, 17–22.

Alfaro, P., Gibert, L., Moretti, M., García-Tortosa, F.J., Sanz de Galdeano, C., Jesús Galindo-Zaldívar, J., López-Garrido, A.C., 2010. The significance of giant seismites in the Plio-Pleistocene Baza palaeo-lake (S Spain). Terra Nova 22, 172–179.

Alfaro, P., Moretti, M., Soria, J.M., 1997. Soft-sediment deformation structures induced by earthquakes (seismites) in Pliocene lacustrine deposits (Guadix–Baza Basin, Central Betic Cordillera). Eclogae Geologica Helvetica 90 (3), 531–540.

Allen, J.R.L., 1982. Sedimentary Structures. Their Character and Physical Basis. Elsevier, New York (663 pp.).

Alonso-Zarza, A.M., Calvo, J.P., 2000. Palustrine sedimentation in an episodically subsiding basin: the Miocene of the northern Teruel Graben (Spain). Palaeogeography Palaeoclimatology Palaeoecology 160, 1–21.

Álvaro, M., Capote, R., Vegas, R., 1979. Un modelo de evolución geotectónica para la Cadena Celtibérica. Acta Geologica Hispánica 14, 172–177.

Ambraseys, N.N., 1988. Engineering seismology. Earthquake Engineering and Structural Dynamics 17, 1–105.

Anketell, J.M., Cegla, J., Dzulynski, S., 1970. On the deformational structures in systems with reversed density gradients. Rocznik Polskiego Towarzystwa Geologicznego 41, 3–30.

Arlegui, L.E., Simón, J.L., Lisle, R.J., Orife, T., 2005. Late Pliocene–Pleistocene stress field in the Teruel and Jiloca grabens (eastern Spain): contribution of a new method of stress inversion. Journal of Structural Geology 27, 693–705.

Arlegui, L.E., Simón, J.L., Lisle, R.J., Orife, T., 2006. Analysis of non-striated faults in a recent extensional setting: the Plio–Pleistocene Concud fault (Jiloca graben, eastern Spain). Journal of Structural Geology 28, 1019–1027.

Atkinson, G., 1984. Simple computation of liquefaction probability for seismic hazard applications. Earthquake Spectra 1, 107–123.

Audemard, F.A., De Santis, F., 2001. Survey of liquefaction structures induced by recent moderate earthquakes. Bulletin of the International Association of Engineering Geology 44, 5–16.

Bhiry, N., Occhietti, S., 2004. Fluvial sedimentation in a semi-arid region: the fan and interfan system of the Middle Souss Valley, Morocco. Proceedings of the Geologists' Association 115, 313–324.

Blair, T.C., 1999. Sedimentary processes and facies of the waterlaid Anvil Spring Canyon alluvial fan, Death Valley, California. Sedimentology 46, 913–940.

Bryant, G., Monegato, G., Miall, A., 2013. An example of liquefaction-induced interdune sedimentation from the early Jurassic Navajo Sandstone, USA. Sedimentary Geology 297, 50–62.

Capote, R., Muñoz, J.A., Simón, J.L., Liesa, C.L., Arlegui, L.E., 2002. Alpine Tectonics I: the Alpine System north of the Betic Cordillera. In: Gibbons, W., Moreno, T. (Eds.), The Geology of Spain. The Geological Society, London, pp. 368–400.

Carrillo, L., Gisbert, J., 1979. Análisis sedimentológico de unos depósitos tipo 'wadi' en el Plio-Cuaternario de Escorihuela (Teruel). Boletín Geológico Y Minero IV, pp. 329–332.

Castilla, R.A., Audemard, F.A., 2007. Sand blows as a potential tool for magnitude estimation of pre-instrumental earthquakes. Journal of Seismology 11, 473–487.

Chamyal, L.S., Khadkikar, A.S., Malik, J.N., Maurya, D.M., 1997. Sedimentology of the Narmada alluvial fan, western India. Sedimentary Geology 107, 263–279.

Clemmensen, L.C., Abrahamsen, K., 1983. Aeolian stratification and facies association in desert sediments, Arran basin (Permian), Scotland. Sedimentology 30, 311–339.

Collinson, J.D., 1996. Alluvial sediments. In: Reading, H.G. (Ed.), Sedimentary Environments. Blackwell Science, pp. 37–82.

Deynoux, M., Kocurek, G., Proust, J.N., 1989. Late Proterozoic periglacial aeolian deposits on the West African Platform, Taoudeni Basin, western Mali. Sedimentology 36, 531–549.

Enos, P., 1977. Flow regimes in debris flow. Sedimentology 24, 133–142.

Ezquerro, L., Lafuente, P., Pesquero, M.D., Alcalá, L., Arlegui, L.E., Liesa, C.L., Luque, L., Rodríguez-Pascua, M.A., Simón, J.L., 2012. Una cubeta endorreica residual Plio-Pleistocena en la zona de relevo entre las fallas de Concud y Teruel: implicaciones paleogeográficas. Revista de la Sociedad Geológica de España 25, 157–175.

Ezquerro, L., Luzón, A., Navarro, M., Liesa, C.L., Simón, J.L., 2014. Climatic vs. tectonic signals in a continental extensional basin (Teruel, NE Spain) from stable isotope ($\delta^{18}O$) and sequence stratigraphical evolution. Terra Nova 26, 337–346.

Ezquerro, L., Moretti, M., Liesa, C.L., Luzón, A., Pueyo, E.L., Simón, J.L., 2016. Controls on space–time distribution of soft-sediment deformation structures: applying palaeomagnetic dating to approach the *apparent recurrence period* of paleoseisms at the Concud Fault (eastern Spain). Sedimentary Geology.

Ezquerro, L., Moretti, M., Liesa, C.L., Luzón, A., Simón, J.L., 2015. Seismites from a well core of palustrine deposits as a tool for reconstructing the palaeoseismic history of a fault. Tectonophysics 655, 191–205.

Fryberger, S.G., Schenk, C.J., 1988. Pin stripe lamination: a distinctive feature of modern and ancient eolian sediments. Sedimentary Geology 55, 1–15.

Fryberger, S.G., Al-Sari, A.M., Clisham, T.J., 1983. Eolian dune, interdune, sandsheet, and siliciclastic sabkha sediments of an offshore prograding sand sea, Dhahran Area, Saudi Arabia. American Association of Petroleum Geologists Bulletin 67, 280–312.

Fryberger, S.G., Hesp, P., Hastings, K., 1992. Aeolian granule ripple deposits, Namibia. Sedimentology 39, 319–331.

Galli, P., 2000. New empirical relationships between magnitude and distance for liquefaction. Tectonophysics 324, 169–187.

Garcés, M., Krijgsman, W., van Dam, J., Calvo, J.P., Alcalá, L., Alonso, A.M., 1999. Late Miocene alluvial sediments from the Teruel area: magnetostratigraphy, magnetic susceptivity, and facies organisation. Acta Geologica Hispánica 32, 171–184.

Gibert, L., Alfaro, P., García-Tortosa, F.J., Scott, G., 2011. Superposed deformed beds produced by single earthquakes (Tecopa Basin, California): insights into paleoseismology. Sedimentary Geology 235, 148–159.

Godoy, A., Moissenet, E., Ramírez, J.I., Olivé, A., Aznar, J.M., Jerez Mir, L., Aragonés, E., Aguilar, M.J., RamírezdelPozo, J., Leal, M.C., Adrover, R., Alberdi, M.T., Giner, J., GutiérrezElorza, M., Portero, J.M., Gabaldón, V., 1983. Mapa Geológico de España 1: 50.000, hoja n° 542 (Alfambra). IGME, Madrid.

Gradziński, R., Jerzykiewicz, T., 1974. Dinosaur- and mammal-bearing aeolian and associated deposits of the Upper Cretaceous in the Gobi Desert (Mongolia). Sedimentary Geology 12, 249–278.

Gutiérrez, F., Gutiérrez, M., Gracia, F.J., McCalpin, J.P., Lucha, P., Guerrero, J., 2008. Plio-quaternary extensional seismotectonics and drainage network development in the central sector of the Iberian Range (NE Spain). Geomorphology 102, 21–42.

Gutiérrez, F., Lucha, P., Guerrero, J., Carbonel, D., Galve, J.P., 2012. A review on Quaternary tectonic and nontectonic faults in the central sector of the Iberian Chain, NE Spain. Journal of Iberian Geology 38, 145–160.

Gutiérrez, M., Peña, J.L., 1976. Glacis y terrazas en el curso medio del río Alfambra (provincia de Teruel). Boletín Geológico y Minero 87, 561–570.

Hilbert-Wolf, H.L., Simpson, E.L., Simpson, W.S., Tindall, S.E., Wizevich, M.C., 2009. Insights into syndepositional fault movement in a foreland basin; trends in seismites of upper cretaceous Wahweap Formation, Kaiparowits Basin, Utah, USA. Basin Research 21, 856–871.

Horowitz, D.H., 1982. Geometry and origin of large-scale deformation structures in some ancient wind-blown sand deposits. Sedimentology 29 (2), 155–180.

Hunter, R.E., 1977. Basic types of stratification in small eolian dunes. Sedimentology 24, 361–387.

IGME, 2012. QAFI: Quaternary Active Faults Database of Iberia. Accessed "DATE", from IGME web site: http://www.igme.es/infoigme/aplicaciones/QAFI/.

Jo, H.R., Rhee, C.W., Chough, S.K., 1997. Distinctive characteristics of a streamflow-dominated alluvial fan deposit: Sanghori area, Kyongsang Basin (Early Cretaceous), southeastern Korea. Sedimentary Geology 110, 51–59.

Kocurek, G., 1986. Origins of low-angle stratification in aeolian deposits. In: Nickling, W.G. (Ed.), Aeolian Geomorphology. Proceedings of the 17th Annual Binghamton Symposium. Allen & Unwin, pp. 177–193.

Kocurek, G., 1996. Desert Aeolian Systems. In: Reading, H.G. (Ed.), Sedimentary Environments: Processes, Facies and Stratigraphy, third ed. Blackwell Science, Oxford, pp. 125–153.

Kocurek, G., Fielder, G., 1982. Adhesion structures. Journal of Sedimentary Research 52, 1229–1241.

Lafuente, P., Arlegui, L.E., Liesa, C., Simón, J.L., 2011. Paleoseismological analysis of an intraplate extensional structure: the Concud fault (Iberian Chain, eastern Spain). International Journal of Earth Sciences 100 (7), 1713–1732.

Lafuente, P., Arlegui, L.E., Liesa, C.L., Pueyo Anchuela, Ó., Simón, J.L., 2014. Spatial and temporal variation of palaeoseismic activity at an intraplate, historically quiescent structure: the Concud fault (Iberian Chain, Spain). Tectonophysics 632, 167–187.

Lafuente, P., Rodríguez-Pascua, M.A., Simón, J.L., Arlegui, L.E., Liesa, C.L., 2008. Sismitas en depósitos pliocenos y pleistocenos de la fosa de Teruel. Revista de la Sociedad Geológica de España 21 (3–4), 133–149.

Liesa, C.L., 2000. Fracturación Y Campos De Esfuerzos Compresivos Alpinos en la Cordillera Ibérica Y El NE Peninsular Ph.D. Thesis University of Zaragoza (760 pp.).

Liesa, C.L., 2011. Fracturación extensional cretácica en la sierra del Pobo (Cordillera Ibérica, España). Revista de la Sociedad Geológica de España 24, 31–48.

Liesa, C.L., Simón, J.L., 2009. Evolution of intraplate stress fields under multiple remote compressions: the case of the Iberian Chain (NE Spain). Tectonophysics 474, 144–159.

Lowe, D.R., 1975. Water escape structures in coarse-grained sediments. Sedimentology 22, 157–204.

Maxwell, T.A., Haynes Jr., C.V., 2001. Sand sheet dynamics and Quaternary landscape evolution of the Selima Sand Sheet, southern Egypt. Quaternary Science Reviews 20, 1623–1647.

Moissenet, E., 1983. Aspectos de la neotectónica en la Fosa de Teruel. In: Comba, J.A., Ríos, J.M. (Eds.), Geología de España, Libro Jubilar vol. II. IGME, Madrid, pp. 427–446.

Moissenet, E., 1989. Les fosses néogenes de la Chaîne ibérique: leur evolution dans le temps. Bulletin de la Societe Geologique de France (Séries 8) 5, 919–926.

Moretti, M., 2000. Soft-sediment deformation structures interpreted as seismites in Middle–Late Pleistocene aeolian deposits (Apulian foreland, southern Italy). Sedimentary Geology 135, 167–179.

Moretti, M., Van Loon, A.J., 2014. Restrictions to the application of 'diagnostic' criteria for recognizing ancient seismites. Journal of Palaeogeography 3, 162–173.

Moretti, M., Alfaro, P., Caselles, O., Canas, J.A., 1999. Modelling seismites with a digital shaking table. Tectonophysics 304, 369–383.

Moretti, M., Soria, J.M., Alfaro, P., Walsh, N., 2001. Asymmetrical soft-sediment deformation structures triggered by rapid sedimentation in turbiditic deposits (Late Miocene, Guadix Basin, Southern Spain). Facies 44, 283–294.

Mountney, N.P., 2006a. Eolian facies models. In: Walker, R.G., Posamentier, H. (Eds.), Facies Models Revisited. SEPM Mem Vol. 84, pp. 19–83.

Mountney, N.P., 2006b. Periodic accumulation and destruction of aeolian erg sequences in the Permian Cedar Mesa Sandstone, White Canyon, southern Utah, USA. Sedimentology 53, 789–823.

Mountney, N.P., Howell, J., 2000. Aeolian architecture, bedform climbing and preservation space in the Cretaceous Etjo Formation, NW Namibia. Sedimentology 47, 825–849.

Mountney, N.P., Thompson, D.B., 2002. Stratigraphic evolution and preservation of aeolian dune and damp/wet interdune strata: an example from the Triassic Helsby sandstone formation, Cheshire Basin, UK. Sedimentology 49, 805–833.

Nemec, W., Steel, R.J., 1984. Alluvial and coastal conglomerates: their significant features and some comments on gravelly mass-flow deposits. In: Koster, E.H., Steel, R.J. (Eds.), Sedimentology of Gravels and Conglomerates. Can. Soc. Petrol. Geol. Memoir Vol. 10, pp. 1–31.

Obermeier, S., 1996. Use of liquefaction-induced features for paleoseismic analysis. An overview of how seismic liquefaction features can be distinguished from other features and how their regional distribution and properties of source sediment can be used to infer the location and strength of Holocene paleo-earthquakes. Engineering Geology 44, 1–76.

Obermeier, S.F., Jacobson, R.B., Smoot, J.P., Weems, R.E., Gohn, G.S., Monroe, J.E., Powars, D.S., 1990. Earthquake-induced liquefaction features in the coastal setting of South Carolina and in the fluvial setting of the New Madrid Seismic Zone. United States Geological Survey Professional Paper 1504 (44 pp.).

Oliveira, C.M.M., Hodgson, D.M., Flint, S.S., 2009. Aseismic controls on *in situ* soft-sediment deformation processes and products in submarine slope deposits of the Karoo Basin, South Africa. Sedimentology 56, 1205–1225.

Opdyke, N., Mein, P., Lindsay, E., Pérez-González, A., Moissenet, E., Norton, V.L., 1997. Continental deposits, magnetostratigraphy and vertebrate paleontology, late Neogene of eastern Spain. Palaeogeography, Palaeoclimatology, Palaeoecology 133, 129–148.

Owen, G., 1987. Deformation processes in unconsolidated sands. In: Jones, M.E., Preston, R.M.F. (Eds.), Deformation of Sediments and Sedimentary Rocks. Geological Society, London, Special Publications Vol. 29, pp. 11–24.

Owen, G., 2003. Load structures: gravity driven sediment mobilization in the shallow subsurface. In: Rensebergen, P.V., Hillis, R.R., Maltman, A.J., Morley, C.K. (Eds.), Subsurface Sediment Mobilization. Geological Society of London, Special Publication Vol. 216, pp. 21–34.

Owen, G., Moretti, M., 2008. Determining the origin of soft-sediment deformation structures: a case study from Upper Carboniferous delta deposits in south-west Wales, UK. Terra Nova 20, 237–245.

Owen, G., Moretti, M., 2011. Identifying triggers for liquefaction-induced soft-sediment deformation in sands. Sedimentary Geology 235, 141–147.

Owen, G., Moretti, M., Alfaro, P., 2011. Recognising triggers for soft-sediment deformation: current understanding and future directions. Sedimentary Geology 235, 133–140.

Papathanassiou, G., Pavlides, S., Christaras, B., Pitilakis, K., 2005. Liquefaction case histories and empirical relations of earthquake magnitude versus distance from the broader Aegean region. Journal of Geodynamics 40, 257–278.

Pavlides, S., Caputo, R., 2004. Magnitude versus faults' surface parameters: quantitative relationships from the Aegean region. Tectonophysics 380, 159–188.

Peña, J.L., Gutiérrez, M., Ibáñez, M.J., Lozano, M.V., Rodríguez, J., Sánchez, M., Simón, J.L., Soriano, M.A., Yetano, L.M., 1984. Geomorfología de la Provincia de Teruel. Instituto de Estudios Turolenses, Teruel (149 p.).

Ramos, A., Sopeña, A., 1983. Gravel bars in low sinuosity streams (Permian and Triassic, Central Spain). In: Collinson, J.D., Lewin, J. (Eds.), Modern and Ancient Fluvial Systems. IAS Spec. Publ. Vol. 6, pp. 301–312.

Roca, E., Guimerà, J., 1992. The Neogene structure of the eastern Iberian margin: structural constraints on the crustal evolution of the Valencia trough (western Mediterranean). Tectonophysics 203, 203–218.

Rodríguez-López, J.P., Clemmensen, L.B., Lancaster, N., Mountey, N., Veiga, G., 2014. Archean to recent aeolian sand systems and their sedimentary record: current understanding and future prospects. Sedimentology 61, 1487–1534.

Rodríguez-López, J.P., Liesa, C.L., Van Dam, J., Lafuente, P., Arlegui, L., Ezquerro, L., De Boer, P.L., 2012a. Aeolian construction and alluvial dismantling of a fault-bounded intracontinental aeolian dune field (Teruel Basin, Spain): a continental perspective on Late Pliocene climate change and variability. Sedimentology 59, 1536–1567.

Rodríguez-López, J.P., Melendez, N., de Boer, P.L., Soria, A.R., 2008. Aeolian sand sea development along the mid-Cretaceous western Tethyan margin (Spain): erg sedimentology and palaeoclimate implications. Sedimentology 55, 1253–1292.

Rodríguez-López, J.P., Meléndez, N., de Boer, P.L., Soria, A.R., 2010. The action of wind and water in a back erg margin system close to the Variscan Iberian Massif. Sedimentology 57, 1315–1356.

Rodríguez-López, J.P., Meléndez, N., de Boer, P.L., Soria, A.R., 2012b. Controls on marine-erg margin cycle variability: aeolian-marine interaction in the mid-Cretaceous Iberian Desert System, Spain. Sedimentology 59, 466–501.

Rodríguez-López, J.P., Meléndez, N., Soria, A.R., Liesa, C.L., Van Loon, A.J., 2007. Lateral variability of ancient seismites related to differences in sedimentary facies (the syn-rift Escucha Formation, mid-Cretaceous, Spain). Sedimentary Geology 201, 461–484.

Rodríguez-Pascua, M.A., Calvo, J.P., De Vicente, G., Gómez-Gras, D., 2000. Soft-sediment deformation structures interpreted as seismites in lacustrine sediments of the Prebetic Zone, SE Spain, and their potential use as indicators of earthquake magnitudes during the Late Miocene. Sedimentary Geology 135, 117–135.

Rubio, J.C., Simón, J.L., 2007. Tectonic subsidence *vs.* erosional lowering in a controversial intramontane depression: the Jiloca basin (Iberian Chain, Spain). Geological Magazine 144, 1–15.

Scherer, C.M.S., 2000. Eolian dunes of the Botucatu Formation (Cretaceous) in southernmost Brazil: morphology and origin. Sedimentary Geology 137, 63–84.

Seilacher, A., 1969. Fault-graded beds interpreted as seismites. Sedimentology 13, 15–159.
Simón, J.L., 1982. Compresión y distensión alpinas en la Cadena Ibérica Oriental Ph.D. Thesis Universidad de Zaragoza. Publ. Instituto de Estudios Turolenses, Teruel (1984) (269 pp.).
Simón, J.L., 1989. Late Cenozoic stress field and fracturing in the Iberian Chain and Ebro Basin (Spain). Journal of Structural Geology 11, 285–294.
Simón, J.L., Arlegui, L.E., Lafuente, P., Liesa, C.L., 2012. Active extensional faults in the central-eastern Iberian Chain, Spain. Journal of Iberian Geology 38, 127–144.
Sims, J.D., 1975. Determining earthquake recurrence intervals from deformational structures in young lacustrine sediments. Tectonophysics 29, 141–152.
Sims, J.D., Garvin, C.D., 1995. Recurrent liquefaction induced by the 1989 Loma Prieta earthquake and 1990 and 1991 aftershocks. Implications for paleoseismicity studies. Seismological Society of America Bulletin 85, 51–65.
Sohn, Y.K., 2000. Coarse-grained debris-flow deposits in the Miocene fan deltas, SE Korea: a scaling analysis. Sedimentary Geology 130, 45–64.
Stanistreet, I.G., Stollhofen, H., 2002. Hoanib River flood deposits of Namib Desert interdunes as analogues for thin permeability barrier mudstone layers in aeolianite reservoirs. Sedimentology 49, 719–736.
Stirling, M., Rhoades, D., Berryman, K., 2002. Comparison of earthquake scaling relations derived from data of the instrumental and preinstrumental era. Bulletin of the Seismological Society of America 92, 812–830.
Thakkar, M.G., Goyal, B., 2004. On the relation between magnitude and liquefaction dimension at the epicentral zone of 2001 Bhuj earthquake. Current Science 87 (6), 811–817.
Turner, P., 1980. Continental red beds. Developments in Sedimentology 29. Elsevier, Oxford (562 pp.).
van Dam, J.A., 1997. The Small Mammals from the Upper Miocene of the Teruel–Alfambra Region (Spain): Paleobiology and Paleoclimatic Reconstructions Ph.D. Thesis University of Utrecht (204 pp.).
van Dam, J.A., Abdul Aziz, H., Álvarez Sierra, M.A., Hilgen, F.J., van den Hoek Ostende, L.W., Lourens, L.J., Mein, P., van der Meulen, A.J., Pelaez-Campomanes, P., 2006. Long-period astronomical forcing of mamal turnover. Nature 443, 687–691.
van Dam, J.A., Alcalá, L., Alonso-Zaraza, A., Calvo, J.P., Garcés, M., Krijgsman, W., 2001. The upper Miocene mammal record from the Teruel–Alfambra region (Spain). The MN system and continental stage/age concepts discussed. Journal of Vertebrate Paleontology 21, 367–385.
van de Weerd, A., 1976. Rodent faunas of the Mio-Pliocene continental sediments of the Teruel–Alfambra region, Spain. Utrecht Micropaleontol. Bulletin, Special Publication 2 (217 pp.).
Vegas, R., Fontboté, J.M., Banda, E., 1979. Widespread neogene rifting superimposed on alpine regions of the Iberian Peninsula. Proceedings symposium evolution and tectonics of the western Mediterranean and surrounding areas, EGS, Viena. Instituto Geográfico Nacional, Madrid, Special Publication 201, 109–128.
Wells, D.L., Coppersmith, K.J., 1994. New empirical relationships among magnitude, rupture length, rupture width, rupture area, and surface displacement. Bulletin of the Seismological Society of America 84, 974–1002.